Influence of viscous dampers ultimate capacity on the seismic reliability of building structures

Fabrizio Scozzese [a], Laura Gioiella [a], Andrea Dall'Asta [a], Laura Ragni [b], Enrico Tubaldi [c]

[a] *SAAD, University of Camerino, Viale della Rimembranza 3, 63100 Ascoli Piceno, Italy*

[b] *Department of Civil and Building Engineering and Architecture, Università Politecnica delle Marche, Via Brecce Bianche, 60131 Ancona, Italy*

[c] *Department of Civil and Environmental Engineering, University of Strathclyde75 Montrose Street, Glasgow G1 1XJ, UK*

ABSTRACT

Anti-seismic devices should be designed with proper safety margins against their failure, because the reliability of the structural system where they are installed is strongly influenced by their reliability. Seismic standards generally prescribe safety factors (reliability factors) amplifying the device responses at the design condition, in order to reach a target safety level. In the case of Fluid Viscous Dampers (FVDs), these factors are applied to the stroke and velocity, and their values are not homogeneous among seismic codes.

This paper investigates the influence of the values of the safety factors for FVDs on the reliability of the devices and of the structural systems equipped with them. An advanced FVD model is employed to account for the impact forces arising when the dampers reach the end-stroke and the brittle failure due to the attainment of the maximum force capacity. The effect of damper failure on both the fragility and the seismic risk of the structural system is investigated by performing multiple-stripe analysis and monitoring different global and local demand parameters. In particular, a parametric study has been carried out, considering two case studies consisting of a low-rise and a medium-rise steel building, coupled with a dissipative system with linear and nonlinear properties and studying the consequences of different values of safety factors for stroke and forces. The study results give evidence to the potential brittle behaviour of the coupled system and provide information about the relationships between damper safety factors and effective structural reliability. Some preliminary suggestions are given on possible improvements of current design approaches and on the values of the reliability factors to be considered for future code revision.

Keywords: energy dissipation; failure; seismic risk and safety; reliability factors; multiple stripe analysis; nonlinear dynamic analysis.

1 INTRODUCTION

Fluid viscous dampers (FVDs) are devices widely used for seismic passive protection of both new and existing structures. They are widely employed for reducing displacements and interstorey drift demands in newly-designed structures as well as in existing ones by using both external and internal configurations [1]-[8].

Several approaches are to date available for designing both size and location of viscous dampers within a building frame based on direct procedures [1][9][10][11][12] or optimization methods [13][14] (see [15] for a thorough review of design strategies for viscous dampers). These design approaches generally allow to control the seismic performance of buildings under the design seismic intensity level. However, the reliability under extreme, low-probability earthquake events may be characterized by low robustness and inadequate safety levels because dampers usually exhibit a brittle collapse behaviour and their failure may trigger the collapse of the whole system. Consequently, the choice of adequate safety factors for the design of the dampers is of paramount importance for obtaining a satisfactory performance under strong actions and controlling the probability of failure.

It is noteworthy that the robustness under extreme loadings is usually not a concern for traditional steel and concrete structures, thanks to their redundant static schemes and ductile material properties, able to redistribute the structural damage. Thus, frame structures generally behave well under exceptional actions, provided that details or connections are adequately designed [16][17][18]. Moreover, procedures to make high quality structural components are consolidated as well as safety coefficients to be used in the design. As a result, while code conforming traditional solutions are characterized by adequate reliability levels, code conforming structures equipped with fluid viscous dampers may show reliability levels below the target suggested by the design codes and the technical literature [19][20][21][22][23].

In order to evaluate the probability of collapse of structures equipped with dampers, risk analyses must be performed by using probabilistic approaches [25]-[33]. Recent probabilistic analyses have investigated some specific issues, such as the effect of ground motion variability on the response of systems equipped with either linear and nonlinear viscous dampers [28][29][30]; the influence of the degree of nonlinearity of the dampers [29][31], and the effect of the damper parameters variability [31][32][33] stemming from the device manufacturing process, as acknowledged by the main international Standards for seismic structural design [19][20][21][22]. However, in these studies the device failure was not explicitly taken into account. Thus, more accurate studies simulating the effect of the device failure should be carried out to provide a better evaluation of the structural reliability under strong earthquakes.

This paper aims to evaluate the consequences of the dissipative device failure on the seismic performance of two benchmark structural systems, by adopting a model describing the brittle failure of the devices due to the attainment of the force capacity, related to the over-velocity or to the achievement of the end-stroke and its influence on the structural reliability. In particular, it is assumed that a brittle failure occurs in the dampers once the maximum force is attained, consistently with the viscous damper numerical model proposed in [34]. The problem is analysed by using a probabilistic approach and by evaluating the mean annual frequency of exceedance of different values of the multiple response parameters related to the performance of dampers and structure. For this purpose, Multi Stripe Analysis (MSA) [35] is carried out and results are given in terms of fragility curves and demand hazard curves for the engineering demand parameters (EDPs) of interest. Fragility analyses of failure of dampers give evidence to the failure sequence and potential lack of robustness of the coupled system.

The two case studies analysed here consist of steel buildings with different dynamic properties, already considered as benchmark cases in previous studies (SAC Phase II Steel Project, [43]). For consistency with the adopted benchmark case studies, the seismic hazard is also assumed equal to the one of [43]. The dissipative system is dimensioned to provide an added damping equal to 30%, using both linear and nonlinear devices, by varying their degree of nonlinearity among three values. The capacity of the dampers (stroke and strength) is evaluated at the design condition, corresponding to a seismic action with Mean Annual Frequency (MAF) of exceeding equal to $2x10^{-3}$.

Some preliminary results under increasing harmonic load histories are reported to illustrate the model capabilities and the sequence of failures triggered by the damper failure. Subsequently, fragility curves and demand hazard curves are illustrated, where the structural performance is analysed considering MAF of exceeding up to 10^{-5} 1/yr. Results obtained by considering different amplification factors for the design of damper parameters are evaluated and compared. In particular, the prescriptions of European codes [20][21] and American Standards [19] are considered. Parametric analysis includes both the case of linear viscous dampers and nonlinear viscous dampers with different nonlinear properties. The case without dampers and the one in which the damper failure is disregarded are also considered for comparison purposes.

The obtained results shed light on the influence of the damper failure on the global reliability of the system and on the effect of the amplification factors on the MAF of failure.

2 FVDS MODELLING AND SEISMIC CODE PROVISIONS

2.1 Fluid viscous dampers modelling

The constitutive law of a fluid viscous damper (FVD) can be described through the following relationship [34][44]:

$$F_d(v) = c|v|^{\alpha} sgn(v) \tag{1}$$

where v is the relative velocity between the device ends, F_d is the damper resisting force, $|v|$ is the absolute value of v, sgn is the sign operator, c and α are two constitutive parameters: the former is an amplification factor, while the latter describes the damper nonlinear behaviour.

It is worth noting that viscous dampers can be produced with α values ranging from 0.1 and 2. Devices with $\alpha > 1$ are not dissipative and are used as shock transmitters. Devices with $0.1 \leq \alpha \leq 1.0$ are all potentially suitable for seismic energy dissipation, among these values, the range $0.3 \leq \alpha \leq 1.0$ is the most widespread [36][37][38][39].

A fluid viscous damper generally consists of a steel cylinder filled of a silicone fluid, within which a steel piston with small orifices on its head can move. In case of seismic events, the fluid is forced to pass through the orifices, moving from one side to the opposite side of the cylinder, thus dissipating into heat the input mechanical energy. The higher is the velocity of the movement, the greater is the dissipated energy. The cylinder is equipped with spherical hinges at its ends to avoid device bending. FVDs are generally connected to the structure by a stiff connection, consisting in a driver brace, dimensioned using an over-strength factor with respect to the viscous device. The stiffness of the driver brace is an important feature, because it needs to be sufficiently high to allow the device to be effective in dissipating energy. Further details on the damper components and their behaviour can be found in [34].

The failure of a damper is related to the exceedance of its strength capacity and can be attained because of the forces related to the end-stroke impact or can be due to excessive piston velocity. According to the described behaviour, dampers are generally classified and tested with reference to two characteristic parameters: the maximum values of stroke $\Delta_{d,max}$, and the maximum transmissible force $F_{d,max}$.

The end-stroke can be attained both in tension (maximum elongation of the device) and in compression (maximum shortening of the device). However, the attainment of an impact does not strictly imply the damper failure because the impact force may be lower than the device strength.

The second mechanism refers to the attainment of the maximum viscous force due to an excessive value of the velocity of the piston (over-velocity with respect to the design value). This extreme value of the force can induce a leak of the fluid or can damage the damper components, resulting in the failure of the device. It is noteworthy that once the maximum capacity $(F_{d,max})$ is attained, the resulting failure mechanisms is brittle, thus making the device ineffective, with no residual ability to sustain loads or dissipate energy.

The model, proposed hereinafter, aims to describe the two aforesaid mechanisms using the damper model, depicted in **Fig. 1**. It is composed of three elements: a dashpot, describing the dissipative behaviour; a hook and gap element, set in parallel to the dissipative device, which simulate the impact due to either excessive shortening ($-\Delta_{d,max}$) or elongation ($+\Delta_{d,max}$); and a third element, set in series with the others, simulating the failure due to the attainment of the force capacity. In this paper, the strength capacity is assumed to be the same in traction and in compression and the failure occurs when the modulus of damper force attains the limit value $F_{d,max}$.

The damper model discussed above is implemented in OpenSees [45] using two-node link elements simulating each of the three components, while various material properties are used to describe the different behaviours. A "Viscous material" is used for the dissipative element, by assigning the values of the constitutive parameters c and α. An "ElasticMultilinear material" depicts the force-displacement relationship related to impacts occurring both for elongation and shortening. Finally, a "MinMax material" is used to simulate the brittle failure, assigning the value of the strength capacity $F_{d,max}$. The stiffness of the "MinMax material" can be used to model the overall deformability of damper, connections, and brace. However, once the strength capacity is reached, the element fails and does not provide any more contribution in terms of reaction force.

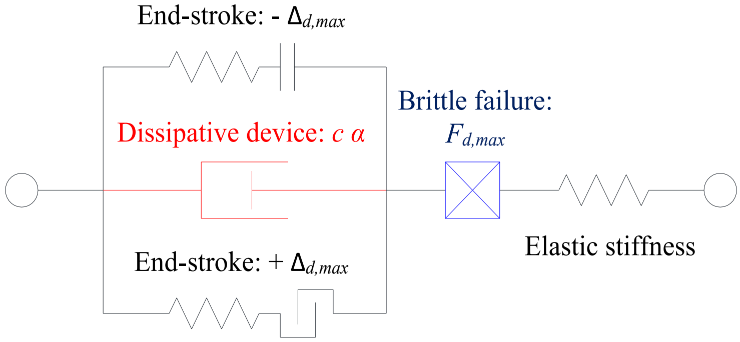

Fig. 1. Dissipative device model encompassing the failure mechanisms

2.2 *International regulatory framework: an overview*

Modern seismic codes prescribe that anti-seismic devices shall be dimensioned starting from the values of the control parameters evaluated for seismic design actions having an assigned probability of exceedance. Then, the capacities of the devices are assigned amplifying these control parameters, which are stroke and force for the FVDs, by means of amplification factors, or reliability factors, in order to ensure a target level of safety. This procedure makes simpler the dimensioning, avoiding an explicit probabilistic analysis considering all the uncertainties of interest. Generally, in the case of dampers, Standards suggest reliability factors that account for uncertainties related to damper response, manufacturing tolerances, ageing phenomena and temperature variations, in addition to uncertainties related to seismic action and structure.

The amplification factors proposed by Codes are two and aim to control the two failure mechanisms discussed above. The former, here denoted by γ_Δ, amplifies the maximum stroke measured at design condition. The amplified stroke must not exceed the damper capacity $\Delta_{d,max}$. The latter, here denoted by γ_v, amplifies the maximum velocity measured at design condition. Damper force is obtained by Eqn. (1) and must not exceed the damper capacity $F_{d,max}$.

In this study we refer to the provisions of US and EU Codes. In the US, the standard for the retrofit of existing buildings (ASCE 41-2017) [19] provides clear indications on the values and applicability of safety factors for viscous dampers. It prescribes that all energy dissipation devices shall be capable of sustaining the force and displacement associated with a velocity equal to 130% ($\gamma_\Delta = \gamma_v = 1.3$) or 200% ($\gamma_\Delta = \gamma_v = 2.0$) of the maximum calculated velocity for that device. The two options depend on the number of devices installed within each storey and each direction of the building and the performance objective assumed [19]. The safety coefficients should be applied to the velocity calculated with a seismic action characterized by an exceedance probability of 5% in 50 years for existing buildings or the Risk-Targeted Maximum Considered Earthquake (MCE) [22] for the new ones. The value of 200% applies only in the case that less than four energy dissipation devices are installed in a given storey along one principal direction of the building, otherwise the coefficient 130% can be used. In the ASCE 41-2017 [19] the property variations of the energy dissipation devices are taken into account through the so called property modification factors (λ factors). These factors define the upper- and lower-bound properties of the devices, accounting for manufacturing tolerances, device characteristics not explicitly considered during testing and environmental effects and aging. The λ factors are not considered in the present work.

In Europe, the reference standards are Eurocode 8 [21] and EN15129 [20], which regulates the devices production and integrates the Eurocode prescriptions concerning design and structural reliability. In the section "General design rules" of EN15129, it is specified that, for anti-seismic devices (seismic isolators excluded), a reliability factor γ_x equal or greater than 1 shall be applied to the effects of the design seismic action on the devices, while an over-strength factor $\gamma_{Rd} = 1.1$ is recommended for designing the connections with the structure. According to Eurocode 8, the design seismic action shall be evaluated considering the Ultimate Limit State (ULS) hazard intensity, characterized by an exceedance probability of 10% in 50 years, corresponding to a MAF of exceedance equal to 2.1×10^{-3}. The value of the reliability factor should be provided by the Eurocodes (as specified in section 4.1.2, note 2 of EN15129), but this information is lacking in the current version. The same EN15129, in the section dedicated to velocity dependent devices, prescribes that the design velocity shall be amplified by a reliability factor $\gamma_v = 1.5$. However, it is worth to observe that no amplification factor is specified for the damper stroke, which means that the stroke capacity could be determined by assuming a γ_Δ factor equal to 1.0. The Italian standard, NTC 2018 [46], is compatible with European codes but its prescriptions are more demanding, requiring that design velocities are amplified by the same reliability factor γ_v given by the EN15129, but prescribes that the response parameters of the devices are evaluated at the Collapse Limit State (seismic actions with exceedance probability of 5% in 50 years). However, similarly to EN15129, no specific indications are given about the damper stroke capacity. Similarly to the US Code [19], also the EN15129 provides tolerance limits (t_d) for velocity dependent devices which are relevant to variations within the supply (statistical variations), as well as variations due to temperature, ageing, etc. These indications regarding the tolerances are also adopted by the Italian NTC 2018 [46] and are not considered in this work.

3 PARAMETRIC ANALYSIS

In this section, a parametric analysis is carried out to understand how the failure of dampers affects the seismic response and performance of steel frame structures. Two different steel moment-resisting frames are considered, representative of low-rise and medium-rise building. The buildings are equipped with FVDs with different non-linearity levels, corresponding to values of the damper exponent α of 1.0, 0.6 and 0.3. Different values of the amplification factors are considered for dampers design. The obtained results are also compared to those corresponding to two limit cases: a) without dampers (bare frame), and b) dampers do not fail.

3.1 Steel buildings frame structures

The two case studies consist of a 3-storey and 9-storey steel moment-resisting frame buildings, designed as part of the SAC Phase II Steel Project, and located in the Los Angeles area. The buildings were designed for gravity, wind, and seismic loads in order to conform to local code requirements and have been widely used as benchmark structure in several studies concerning structural response control (e.g., [2][43][29][47]). **Fig. 2** illustrates the structural system of the buildings, consisting of perimeter moment-resisting frames and internal gravity frames with shear connections. The numerical model of the buildings consists only in a two-dimensional frame, representing one half of the structure in the north–south direction, which is the short and also the weak direction of the buildings. **Fig. 2** also shows the main geometrical details and dimensions of the steel members (wide-flange sections are used for both columns and beams), together with the locations of the fluid viscous dampers, whose design is described in section 3.3. Further details concerning the structural geometry and loads can be found in [47].

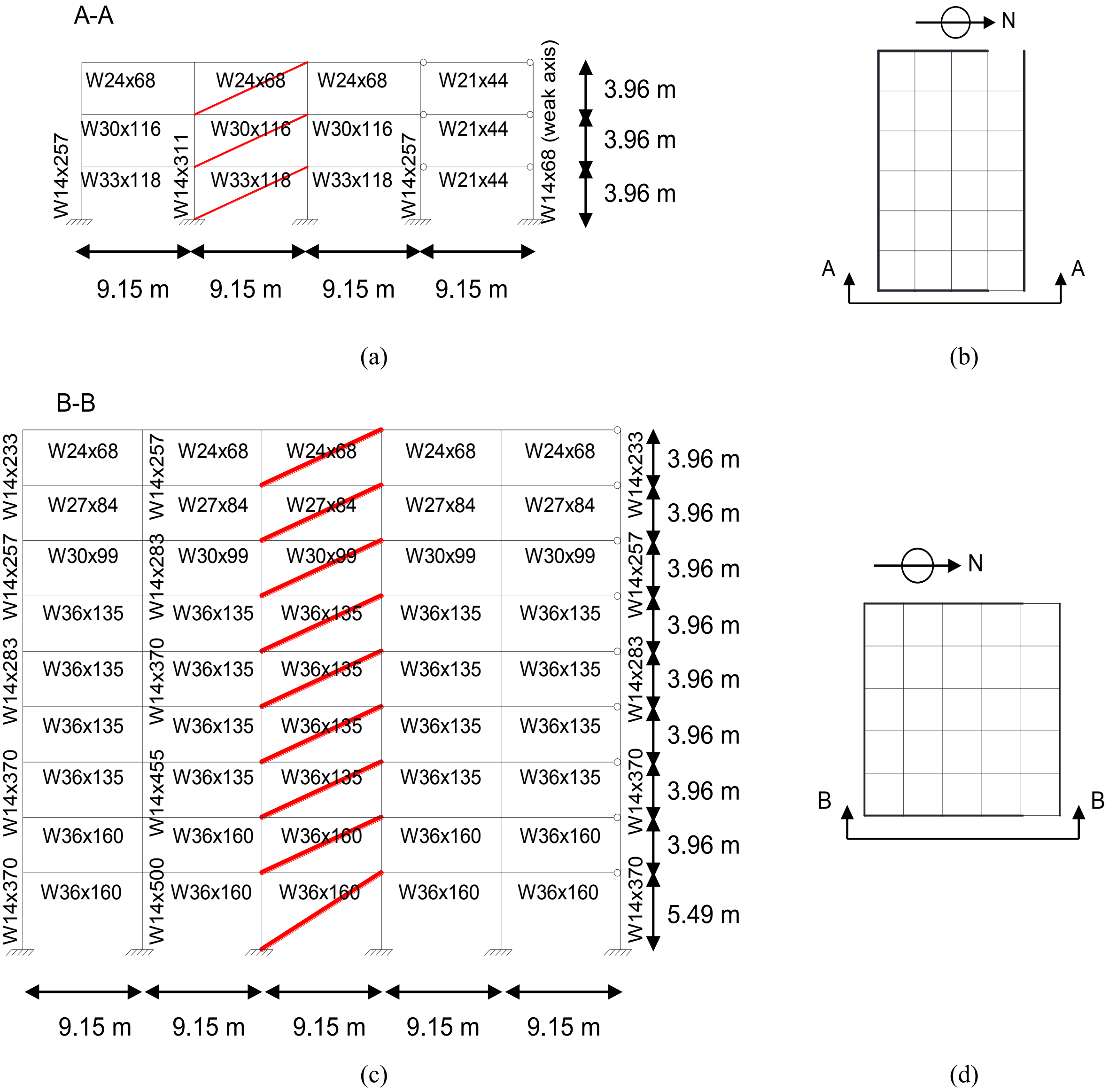

Fig. 2. Case studies: (a) elevation (red lines highligth FVDs location) and (b) plan (thick lines highlight moment-resisting frames) of 3-storey frame; (c) elevation and (d) plan of 9-storey frame.

The finite element models of the systems are developed in OpenSees [45] following the same methodology described in [29] and briefly recalled below. A distributed plasticity approach is adopted [48][49], with nonlinear force-based elements and fibre sections with *Steel02* uniaxial material, accounting for the hysteretic behaviour of the members. A corotational approach for the system coordinate transformation is used to perform large displacement (small strain) analysis and thus account for the nonlinear geometrical effects, whereas an elastic fictitious P-delta column is introduced to consider the vertical loads carried by the inner gravity frames (not explicitly modelled). The strength and deformability of panel zones are neglected. The inherent damping properties are accounted through the Rayleigh model by assigning a 2% damping ratio at the first and second vibration modes. **Table 1** reports, for both the bare buildings, the first three estimated vibration periods T_i, together with the related mass participant factors normalized with respect to the total mass, (MPF_i).

Table 1. Vibration periods for the bare 3-storey and 9-storey steel moment-resisting frame.

3-storey case study			9-storey case study		
Mode	T_i [s]	MPF_i	Mode	T_i [s]	MPF_i
1	0.995	0.827	1	2.225	0.828
2	0.325	0.136	2	0.836	0.109
3	0.173	0.037	3	0.481	0.038

3.2 Seismic hazard

For consistency with the adopted benchmark case studies, the hazard model and the related intensity measure (*IM*) hazard curves are taken from [43]; in the present work, however, the curves have been slightly extrapolated (from 10^{-4} up to almost 10^{-5} 1/year) to make sure that the system failure probabilities can be accurately estimated, by following the recommendation of [42] about the optimal *IM* curve truncation for an accurate risk estimation via MSA analysis.

The spectral pseudo-acceleration $S_a(T_1)$ of a linear elastic SDOF system with 2% damping ratio and fundamental vibration period equal to that of the structure T_1 is considered as intensity measure. Such *IM* also represents the basis of the current seismic hazard maps and building code practice [50]. **Fig. 3** illustrates the hazard curves corresponding to the chosen *IM*, for the three-storey and the nine-storey building frames. The *IM* levels at which MSA is performed are 20 (highlighted by circles in **Fig. 3**), whose corresponding values of MAFs of exceedance and spectral accelerations are summarised in **Table 2**. The *IM* values corresponding to the main limit states suggested by codes are identified by red circles, and they correspond to seismic events with exceedance probability of 50%, 10% and 2% in 50 years.

The record-to-record variability effects are taken into account in the analyses by considering the set of 60 records used in the SAC project [2]. These records are characterized by different seismic intensities, frequency content, and duration. At each intensity level, a subset of 30 ground motions is taken from this set, with *IM* values closest to the considered *IM* level, in order to minimize the scaling procedure operated for making the samples conditional to the *IM*. Further details and features of these records can be found in [2].

For what concerns the FVDs design, this is carried out by considering the set of 30 records corresponding to a MAF of exceedance $\nu_{design} = \nu_{IM}(im_{design}) = 0.0021$ 1/yr (probability of exceedance of 10% in 50 years), associated to the intensities $im_{design} = 0.8866\ g$ for the three-storey frame and $im_{design} = 0.3676\ g$ for the nine-storey frame (g is the gravity acceleration).

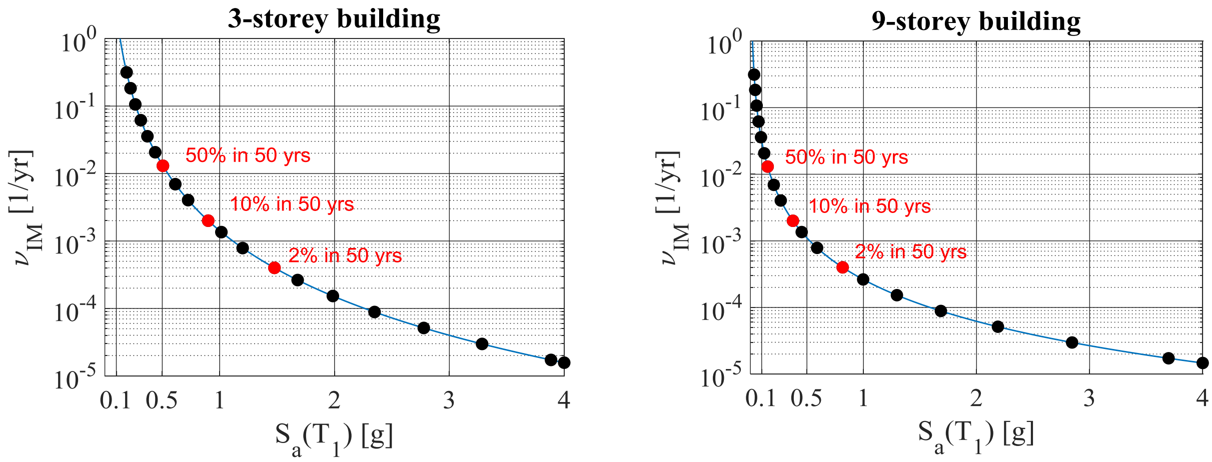

Fig. 3. *IM* hazard curves for the 3- and 9-storey buildings.

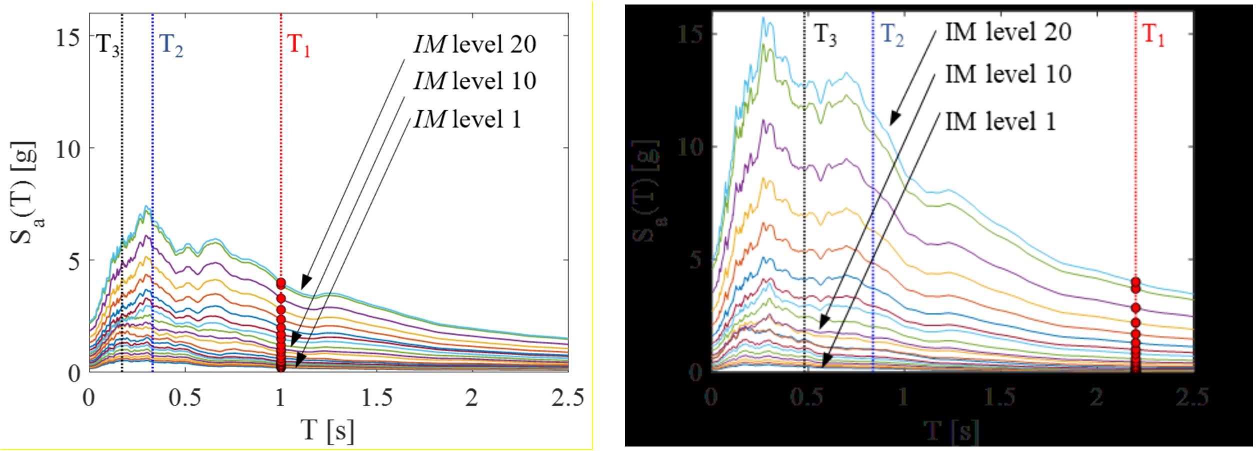

(a) (b)

Fig. 4. Ground motion response spectra averaged at every intensity level: (a) 3-storey; (b) 9-storey.

Table 2. Correspondence between *IM* levels, MAFs and spectral accelerations (in *g*).

IM levels	1	2	3	4	5	6	7	8	9	10
MAF ν_{IM} [1/year]	3.2E^{-1}	1.8E^{-1}	1.1E^{-1}	6.2E^{-2}	3.6E^{-2}	2.1E^{-2}	1.3E^{-2}	7.0E^{-3}	4.0E^{-3}	2.0E^{-3}
3-storey $S_a(T_1$=1.0)	0.19	0.22	0.27	0.31	0.37	0.44	0.48	0.61	0.73	0.90
9-storey $S_a(T_1$=2.2)	0.03	0.04	0.06	0.07	0.09	0.12	0.14	0.21	0.27	0.38
IM levels	11	12	13	14	15	16	17	18	19	20
MAF ν_{IM} [1/year]	1.4E^{-3}	7.9E^{-4}	4.0E^{-4}	2.6E^{-4}	1.5E^{-4}	8.9E^{-5}	5.1E^{-5}	3.0E^{-5}	1.7E^{-5}	1.6E^{-5}
3-storey $S_a(T_1$=1.0)	1.01	1.20	1.48	1.68	1.99	2.35	2.78	3.28	3.89	4.00
9-storey $S_a(T_1$=2.2)	0.45	0.59	0.82	1.00	1.30	1.68	2.19	2.85	3.70	4.00

3.3 Damping systems

The design of the FVDs is carried out to enhance the buildings performance under a seismic scenario with a 10% probability of exceedance in 50 years (ULS scenario according to Eurocode 8). To this aim, a target value $\xi_{add} = 30\%$ has been chosen for supplemental damping. It is worth noting that a damping ratio higher than 30% is usually not recommended because it may lead to a too significant modification of the natural dynamic properties of the building, with potentially detrimental effects in terms of absolute accelerations ([2][15][51]). For this reason, the value of 30% is assumed to investigate an upper bound of the retrofitting scenarios with passive seismic protection strategies. This value is expected to lead to the worst consequences in case of dampers failure.

Dampers design is initiated under the hypothesis of linear viscous behaviour (α = 1.0); constants c_j required to achieve the target damping ratio ξ_{add} are thus calculated for each building storey using the general formula proposed by the ASCE/SEI-41 [19]:

$$\xi_{add} = \frac{T \sum_j c_j f_j^2 \phi_{rj}^2}{4\pi \sum_i m_i \phi_i^2} \tag{2}$$

where the index $j = 1, \dots, n$ denotes the j-th device, T is the period of the first vibration mode of the building; f_j is a magnification factor related to the installation scheme of dampers; ϕ_{rj} the first modal relative displacement between the ends of the damper j in the horizontal direction; m_i is the mass of the i-th storey and ϕ_i is the horizontal first modal displacements of the i-th storey.

In the present study, the dampers are installed in a diagonal arrangement, therefore f_j=cosθ, where θ is the angle between the horizontal direction and the j-th diagonal brace. Moreover, the damping coefficients of the linear devices have been distributed proportionally to the storey shear force of the first mode of the bare frame. As suggested in [9], the relation between the damping coefficient of a single storey, c_j, and the total damping of the building, $\sum_i c_i$ can be expressed as:

$$c_j = \left(V_j \Big/ \sum_i V_i \right) \sum_i c_i \quad (3)$$

where V_j is the shear force of the j-th storey. By substituting Eqn. (3) into Eqn. (2), it is possible to achieve the total supplemental damping ξ_{add} as:

$$\xi_{add} = \frac{T \sum_j \left[V_j (\sum_i c_i) \left(cos\theta_j \phi_{rj} \right)^2 \right]}{4\pi (\sum_i m_i \phi_i^2)(\sum_i V_i)} \quad (4)$$

Eqn. (4) can be rearranged to find the total damping coefficient of the structure, $\sum_i c_i$, and the damping coefficient at the j-th storey can be finally expressed as:

$$c_j = \frac{4\pi \xi_{add} V_j \sum_i m_i \phi_i^2}{T \sum_i V_i \, (cos\theta_i \phi_{ri})^2} \quad (5)$$

Having determined the damping coefficients of the devices for the linear case, the viscous coefficients for the nonlinear FVD corresponding to given value of the exponent α, are evaluated following the approach outlined in [9],[52],[53] and based on the equivalence of the energies dissipated by the linear and nonlinear FVDs. For this purpose, seismic analyses of the system with linear devices are carried out under a set of 30 recorded ground motions, scaled to the design intensity level (i.e., exceedance probability of 10% in 50 years) as discussed in the previous chapter. The mean response in terms of roof displacement of the building, A, is then used to determine the equivalent nonlinear damping coefficients through the following general expression:

$$\xi_{add} = \frac{T^{2-\alpha} \sum_j c_j \lambda f_j^{1+\alpha} \phi_{rj}^{1+\alpha}}{(2\pi)^{3-\alpha} A^{1-\alpha} \sum_i m_i \phi_i^2} \quad (6)$$

where ϕ_i is the modal displacement shape normalised to a unit value at the roof and λ is given by the following expression:

$$\lambda = 2^{2+\alpha} \frac{\Gamma^2(1 + \alpha/2)}{\Gamma(2 + \alpha)} \quad (7)$$

in which Γ is the gamma function.

Eqn. (6) can be specialized to the case of dampers with viscous constant distributed proportionally to the storey shear force of the first mode of the bare frame, installed in a diagonal arrangement. It can be then rearranged to obtain the nonlinear damping coefficient c_j at each elevation, as:

$$c_j = \frac{\xi_{add} (2\pi)^{3-\alpha} A^{1-\alpha} V_j \sum_i m_i \phi_i^2}{T^{2-\alpha} \sum_i V_i \lambda cos\theta_i^{1+\alpha} \phi_{ri}^{1+\alpha}} \quad (8)$$

Table 3 and **Table 4** report the properties of the dissipative devices, c_j and α, for the 3-storey and 9-storey buildings, respectively, for the various levels of dampers nonlinearity considered. It is noteworthy that the maximum interstorey drift along the building height, averaged over the 30 records considered, is equal to 3% and 2.1% respectively for the three-storey and nine-storey bare frames. With the addition of the dampers, they become respectively 1.2% and 1.0%.

Table 5 and **Table 6** report the values of mean displacement $\Delta_{d,j}$, force $F_{d,j}$ and velocity v_j demand for the dampers, evaluated at the design condition. These values result in a probability of failure of the dampers of about 50% under the design earthquake level, if no amplification factors are considered for the damper response parameters.

Table 3. 3-storey building damping properties for different levels of damper nonlinearity.

Case study	α	Floor 1 c_1	Floor 2 c_2	Floor 3 c_3
		$[kNs^{\alpha}/m^{\alpha}]$		
3-storey	1	13,780	11,914	7428
	0.6	7477	6465	4031
	0.3	4669	4037	2517

Table 4. 9-storey building damping properties for different levels of damper nonlinearity.

Case study	α	Floor 1 c_1	Floor 2 c_2	Floor 3 c_3	Floor 4 c_4	Floor 5 c_5	Floor 6 c_6	Floor 7 c_7	Floor 8 c_8	Floor 9 c_9
						$[kNs^{\alpha}/m^{\alpha}]$				
9-storey	1	48,103	46,834	44,578	41,282	36,918	31,534	25,199	17,903	9675
	0.6	17,506	17,044	16,233	15,024	13,435	11,476	9171	6515	3521
	0.3	8133	7899	7518	6962	6226	5318	4250	3019	1632

Table 5. 3-storey building damper design parameters at the design condition.

	3-storey building								
α	Floor 1 $\Delta_{d,1}$ [mm]	Floor 2 $\Delta_{d,2}$ [mm]	Floor 3 $\Delta_{d,3}$ [mm]	Floor 1 $F_{d,1}$ [kN]	Floor 2 $F_{d,2}$ [kN]	Floor 3 $F_{d,3}$ [kN]	Floor 1 v_1 [m/s]	Floor 2 v_2 [m/s]	Floor 3 v_3 [m/s]
1.0	35.4	44.5	37.1	3109	3336	1956	0.23	0.28	0.26
0.6	32.4	41.7	35.6	3090	3050	1824	0.23	0.29	0.27
0.3	29.6	39.7	35.7	3044	2796	1712	0.24	0.29	0.28

Table 6. 9-storey building building damper design parameters at the design condition.

		9-storey building								
		Floor 1	Floor 2	Floor 3	Floor 4	Floor 5	Floor 6	Floor 7	Floor 8	Floor 9
α=1	$\Delta_{d,j}$[mm]	38.4	32.7	31.9	31.9	29.5	27.8	28.7	29.9	24.3
	$F_{d,j}$ [kN]	7781	6060	5416	5075	4379	3930	3559	3011	1614
	v_j [m/s]	0.16	0.13	0.12	0.12	0.12	0.12	0.14	0.17	0.17
α=0.6	$\Delta_{d,j}$ [mm]	38.4	32.3	31.0	31.3	28.3	26.6	28.9	30.2	24.4
	$F_{d,j}$ [kN]	6580	5461	4900	4571	3914	3385	3016	2370	1307
	v_j [m/s]	0.20	0.15	0.14	0.14	0.13	0.13	0.16	0.19	0.19
α=0.3	$\Delta_{d,j}$ [mm]	38.7	32.4	31.3	30.8	28.7	26.1	29.1	31.0	25.8
	$F_{d,j}$ [kN]	5244	4688	4345	4014	3546	2952	2507	1920	1062
	v_j [m/s]	0.23	0.18	0.16	0.16	0.15	0.14	0.17	0.22	0.24

3.4 Amplification factors

Per each value of the constitutive parameter α and per each case-study, five combinations of amplification factors relevant to damper stroke and strength are considered. It is worth to recall that the probability of exceedance of the seismic action suggested by the standards for the dampers design is not homogeneous (10% in 50 years for the European codes and 5% in in 50 years for the existing buildings or the MCE for the new ones in the American code). In order to compare results, the same design action has been considered in the parametric analysis. More precisely, the design action has an annual probability of exceedance equal to 2.1×10^{-3} and it coincides with the action suggested by European Standards.

In detail, γ_v and γ_Δ denote the amplification factors relevant to velocity and stroke, respectively. The first case analysed, (case $\gamma_v = \gamma_\Delta = 1.0$), considers the response parameters reported in **Table 5** and **Table 6** for the design, without applying any amplification through safety factors. Three more cases are analysed: "$\gamma_v = 1.5$ and $\gamma_\Delta = 1.0$" where the displacement is not amplified, while the force is associated with a velocity equal to $\gamma_v = 1.5$ times the maximum one; "$\gamma_v = \gamma_\Delta = 1.5$" where the displacement is amplified with a coefficient equal to $\gamma_\Delta = 1.5$, while the force is associated with a velocity equal to $\gamma_v = 1.5$ times the maximum one; "$\gamma_v = \gamma_\Delta = 2.0$" where the displacement is amplified with a coefficient equal to $\gamma_\Delta = 2.0$, while the force is associated with a velocity equal to $\gamma_v = 2.0$ times the maximum one.

Moreover, one more case is considered that accounts for larger amplification factors: "$\gamma_v = \gamma_\Delta = 3.0$" where the displacement is amplified with a coefficient equal to $\gamma_\Delta = 3.0$, while the force is associated with a velocity equal to $\gamma_v = 3.0$ times the maximum one. Finally, for comparison purposes, two more limit cases are considered: "No Failure" that is the case where no dampers' failures are permitted, and "Bare Model", which represents the frame without FVDs.

3.5 Probabilistic framework

A conditional probabilistic approach is used to estimate, for each case study, the demand hazard functions $\nu_D(d)$ of the random variable D describing the main parameters characterizing the seismic response of the structural systems. The stages needed to estimate $\nu_D(d)$ by a conditional probabilistic approach are: *i*) evaluation of the hazard function $\nu_{IM}(im)$, i.e., the MAF of exceeding the value *im* of the intensity measure *IM*; *ii*) construction of a probabilistic demand model, expressed by the function $G_{D|IM}(d|im)$, linking the generic demand D with the *IM* and expressing the probability of exceeding the demand value d conditional to the seismic intensity level *im*; *iii*) estimation of the mean annual rate of exceedance $\nu_D(d)$ by solving the following convolution integral between the seismic hazard function ν_{IM} and the conditional demand $G_{D|IM}$.

$$\nu_D(d) = \int_{IM} G_{D|IM}(d|im)\,|d\nu_{IM}| \tag{9}$$

In this study, the standard trapezoidal rule is used to solve the integral of Eq. (9), while Multy-Stripes Analysis (MSA) is employed to build the $G_{D|IM}$ function, which requires performing a number (n_{sim}) of nonlinear dynamic structural analyses at discrete *IM* levels (n_{IM}). In order to achieve accurate risk estimations, the number of *IM* levels used to perform MSA is set equal to 20, and at each *IM* level the 30 ground motions with the closest *IM* values are selected and scaled to that *IM* level. This approach, yielding different ground motion combinations for the different *IM* levels considered, permits to avoid excessive scaling of the records. The choice of the values of n_{sim} (30) and n_{IM} (20) is based on the results of a recently proposed study [35], in which an extensive parametric analysis was performed to assess the influence of the main parameters governing MSA on the accuracy of the risk estimates.

4 EFFECTS OF FVDS FAILURE ON THE BENCHMARK STRUCTURES RESPONSE

Before illustrating the results of the probabilistic analyses in detail, it is useful to provide a first insight on the dynamic behaviour following the damper failures. FVDs failures are explicitly modelled based on section 2.1.

In the following, the results obtained for a sinusoidal ground motion of increasing intensity striking the three-storey building are presented first. Successively, the seismic response is discussed, considering some ground motions selected from the MSA analysis. Finally, a preliminary and qualitative evaluation of the overall probabilistic response of the three-storey case-study is proposed.

Analysis results highlight some typical issues related to the damper failures, such as the domino effect on dampers at different storeys, acceleration peaks due to end-stroke impacts, and overall brittle behaviour of the system.

4.1 System response under an increasing sinusoidal input

In this subsection, the results obtained for a sinusoidal ground motion of increasing intensity striking the 3-storey building are presented. The FVDs response parameters at the design condition refer to linear devices ($\alpha = 1$) and to the case "$\gamma_v = \gamma_\Delta = 1.0$". The choice of an increasing harmonic input motion is motivated by the fact that it allows to easily identify the attainment of the damper strength capacity through one of the two mechanisms, impact and over-velocity and the related consequences on the frame undergoing a more general time-history input motion.

Fig. 5 shows the sinusoidal input having a period of 0.9 seconds and an initial magnitude of $1\,m/s^2$. The amplitude of the motion is constant for five cycles, after that it is increased with a coefficient equal to 1.5 and remains again constant for five cycles. The magnification of the motion amplitude is repeated four times, resulting in a motion that has five different amplitudes, with a maximum equal to $5\,m/s^2$, and that lasts 22.5 seconds. At the end of the input, there are few seconds, which are useful to understand how the case study restores its rest condition.

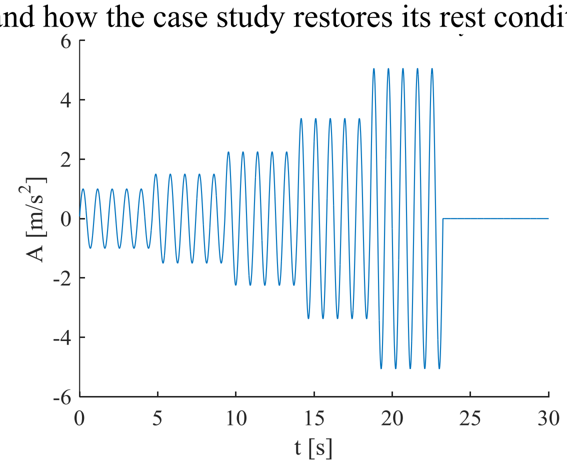

Fig. 5. Sinusoidal incremental dynamic input

Fig. 6 a) - **Fig. 6** h) show the response in terms of damper forces and strokes, $F_{d,i}$ and $\Delta_{d,i}$. floor displacements u_i, floor relative velocities $v_{r,i}$ and floor absolute accelerations A_i. In particular, **Fig. 6** a) and b) illustrate the time-history of the damper forces $F_{d,i}$ recorded along the height of the building. The black solid line refers to the device installed between the ground and the first floor, the red one refers to the intermediate device at the second storey, while the blue one represents the damper at the top storey. At the beginning of the third increment of the sinusoidal input (between 14.4 and 14.5 seconds), graphs show some small ripples, which are more evident for the intermediate and top-storey devices (**Fig. 6** b), and they are caused by small impacts due to the end-stroke attainment. In this case, the impact occurs but it does not lead to the attainment of the damper strength capacity. At the time instant 14.6 s the damper placed at the first level reaches its force capacity due to over-velocity and its force drops to zero. Few instants later, also the other devices fail for over-velocity. These effects can be deeper investigated through **Fig. 6** c) - e), where the stroke-force relationship of each device is shown. In particular, by observing the stroke-force relationships of Fig. 5 c) - e) it is evident that at the beginning of the third increment of the input motion, all the three dampers experience the end-stroke attainment without failure, with impacts that are more evident for the intermediate and top-storey devices. After these impacts, occurred without consequences, the FVDs restore their behaviour as pure dissipative devices. Few instants later, suddenly, the damper located at the ground floor fails due to over-velocity, triggering the sequence of damper failures at the upper elevations. The sequence is highlighted by a series of ripples in the stroke-force relationship of the intermediate and especially top-storey device. The ripples begin when the first device fails and last until all the devices fail for over-velocity.

Fig. 6 f) - h) shows the time-histories of the parameters strictly related to the frame response, highlighting the consequences of the damper failures on the frame itself. Generally, the responses in terms of displacements, relative velocities and absolute accelerations are significantly amplified by the impacts occurring in the dampers and by their failure. The absolute accelerations are more affected than the displacements. It is worth to note that the peaks in terms of absolute accelerations, recorded between 14 and 15 seconds, are mainly related to the impacts experimented by the devices before their failure.

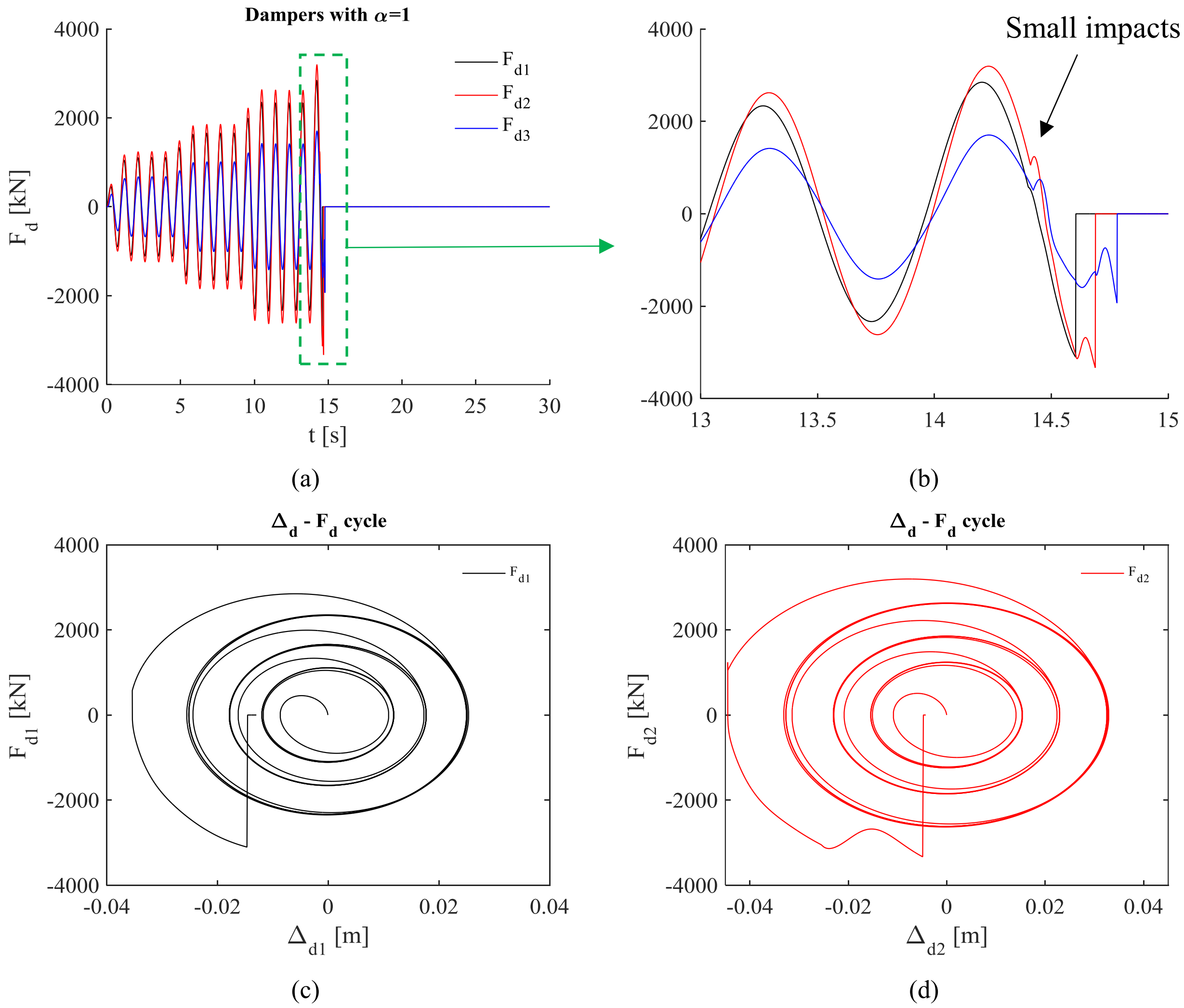

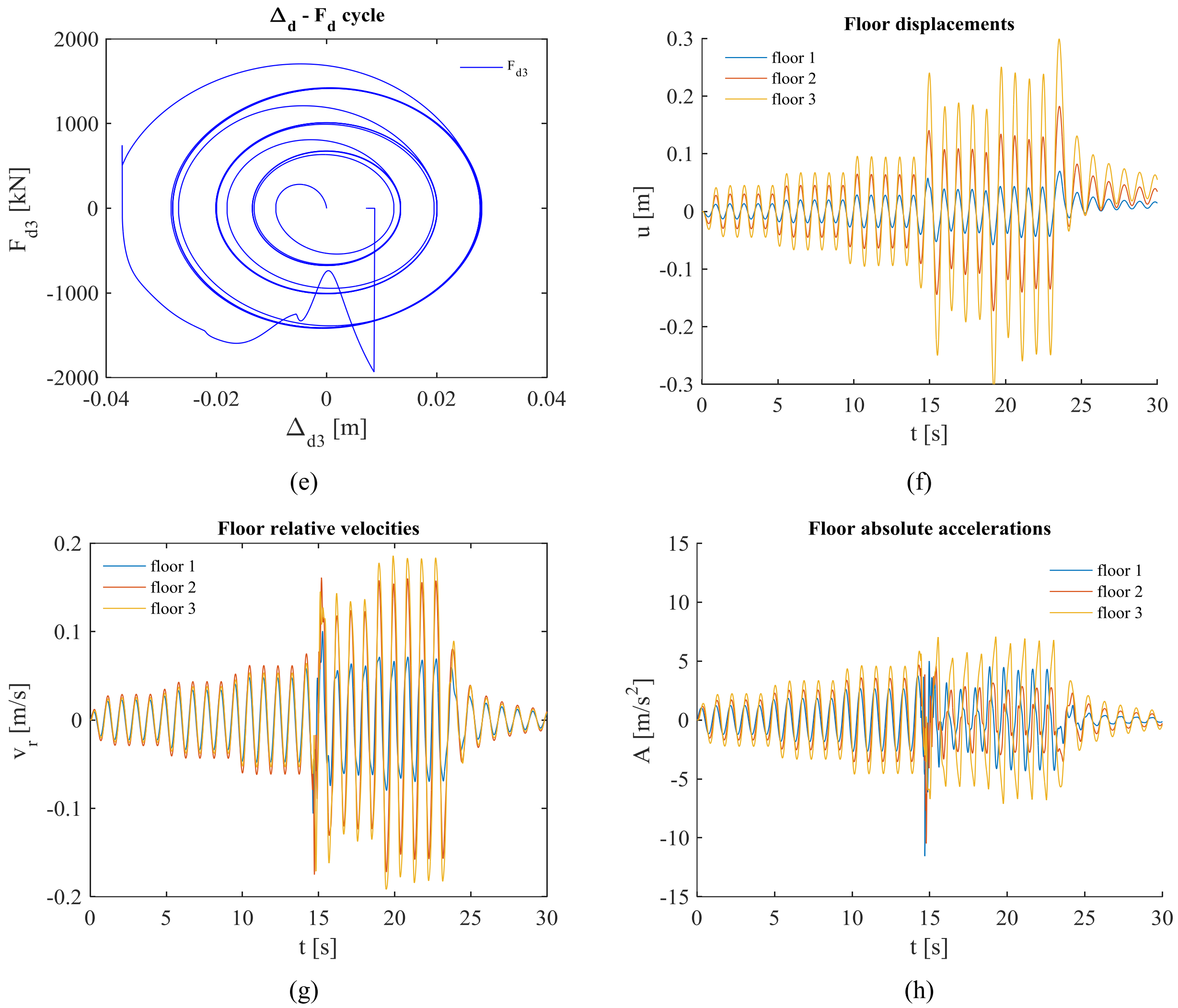

Fig. 6. Dampers response and time histories of different local and global EDPs under harmonic increemental dynamic input

4.2 Three-storey building and nine-storey building seismic response overview

In this subsection, few selected information from MSA analysis are shown to illustrate overall the problem of damper failure and related effects on the structural performance of the three-storey and nine-storey building case studies.

To shed further light on the consequences of FVDs failure, the time-histories of the interstorey-drift ratio (IDR) response of the bare model and of the system with (linear and nonlinear) dampers designed without amplification factors ($\gamma_v = \gamma_\Delta = 1.0$) are compared in **Fig. 7**. Comparison is performed at both low (*IM* level 5) and high (*IM* level 15) seismic intensities and for a single time-history (TH) analysis (TH 17). For sake of brevity and given the high similarity of the response at all floors the response in terms of IDR at floor 1 is only discussed. It is confirmed that at lower seismic intensities FVDs are effective in damping the response (by also reducing residual drift) and that the beneficial response mitigation provided by the dampers vanishes at higher *IM*s, due to the device failure. More specifically, it can be observed that dampers fail at around 4.0 seconds since the beginning of the time-history of *IM* level 15. This is detailed in the inset of **Fig. 7** (b) (close-up plot between 2 and 6 seconds), showing that the IDR response (with both linear and nonlinear devices) is damped until the 4.0 s and then tends towards the bare-frame response; on the contrary, at *IM* level 5 the response of the frame with FVDs is damped over the whole earthquake duration, since no device failure is observed at this intensity level.

For sake of completeness, the dampers force-stroke cyclic responses corresponding to the aforesaid cases (plotted in **Fig. 7**) are shown in **Fig. 8** (*IM* level 5) and **Fig. 9** (*IM* level 15). In each figure a comparison is made between the responses of the linear (red dashed line) and nonlinear dampers (blue dotted line) at the first (figure a) and third storey (figure b). The attainment of the end-stroke (impact) is characterised by a sudden rise in force (with no increase of displacement) while the attainment of the maximum force capacity (hence the failure) can be identified because the force suddenly becomes null and the hysteretic cycle is interrupted. It can be noted that at *IM* level 5 failure is never attained, and thus complete cycles can be observed in **Fig. 8**.

On the contrary, at *IM* level 15 failure occurs on the dampers of both storeys 1 (**Fig. 9**a) and 3 (**Fig. 9**b), corresponding to the cycle's sudden interruption. More in detail, in **Fig. 9**a (floor 1) the failure is achieved with no sign of impact (for both linear and nonlinear dampers); differently, in **Fig. 9**b (floor 3), the force of the linear damper (red line) increases abruptly and immediately after drops to zero, meaning that the impact is responsible for the failure.

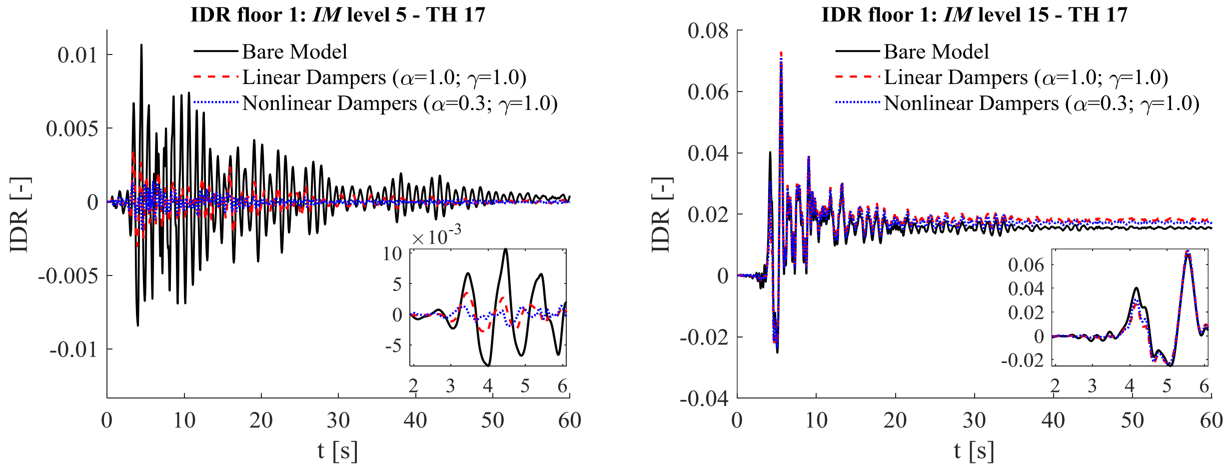

(a) (b)

Fig. 7. Time histories of the IDR at two different *IM* levels (a) *IM* n. 5 and (b) 15. Comparison between the bare model and the model with linear and nonlinear dampers (withouth amplification factors).

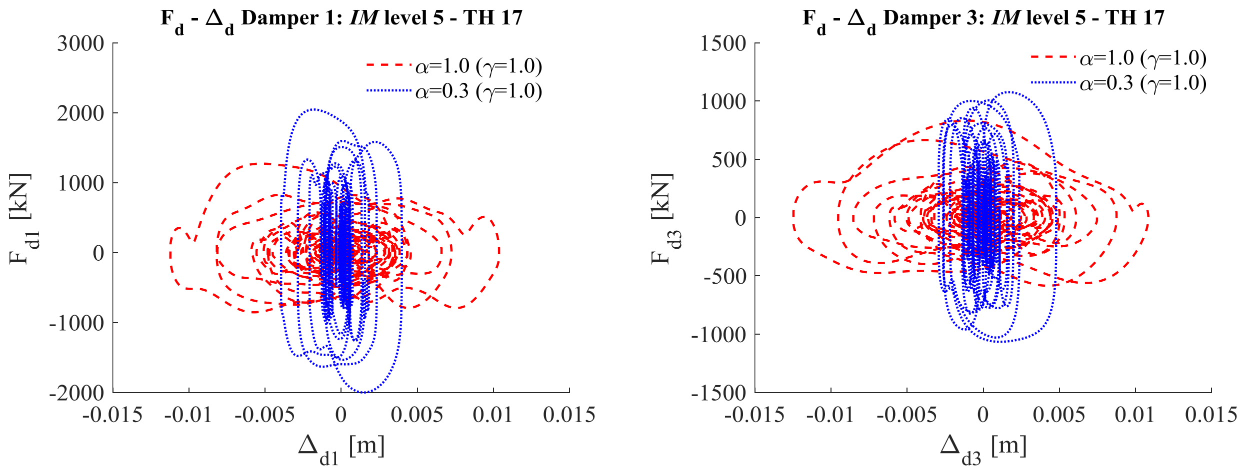

(a) (b)

Fig. 8. Damper response at *IM* levels 5. Comparison between linear and nonlinear dampers (withouth amplification factors) at (a) first and (b) third floor.

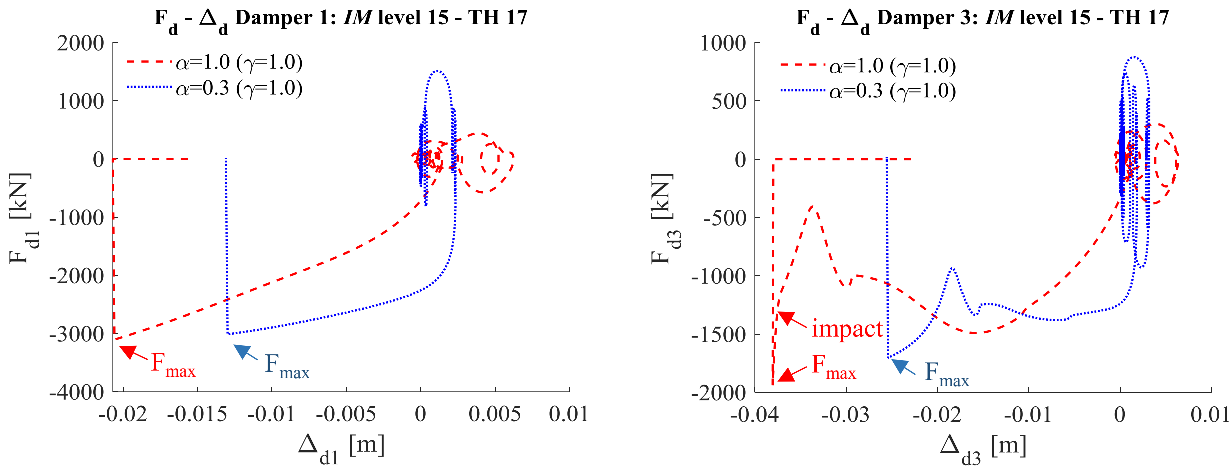

(a) (b)

Fig. 9. Damper response at *IM* levels 15. Comparison between linear and nonlinear dampers (withouth amplification factors) at (a) first and (b) third floor.

In **Fig. 10**, time histories (selected from *IM* level 15) of the force on dampers at different floors are compared. Here dampers failure occurs at 4.0 s, when the forces suddenly drop to zero and the dampers become ineffective. It can be also observed that failure involves devices at all the storeys quite simultaneously.

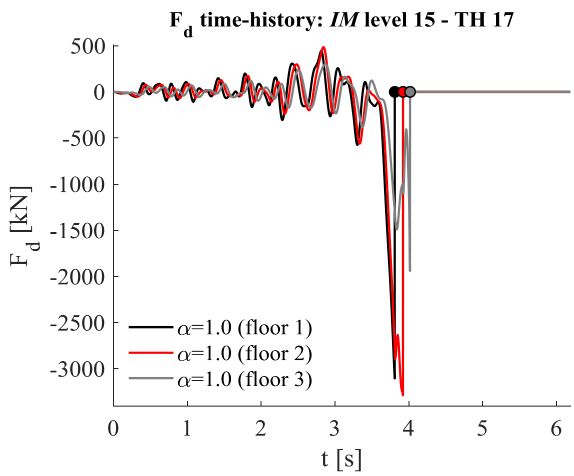

Fig. 10. Failure time-lag among dampers at different floors.

For what concerns the seismic response of the nine-storey building, the differences between the seismic response of this structural system and the previous low-rise building are highlighted in the following. **Fig. 11** a) shows the time-history of the forces at the various levels under record #17 scaled to the *IM*=15 (with intensity 2.0 *g*, 2.26 times higher than the design seismic intensity). Although damper failure initiates at the bottom storey, it propagates quite rapidly to the devices placed at the higher levels. However, damper failure can also propagate from the top to the bottom of the building, as observed by the response shown in **Fig. 11** b), related to the same record scaled to *IM*=10 (design seismic intensity). In general, it is observed that when one device fails, all the other devices fail too, even though at different times.

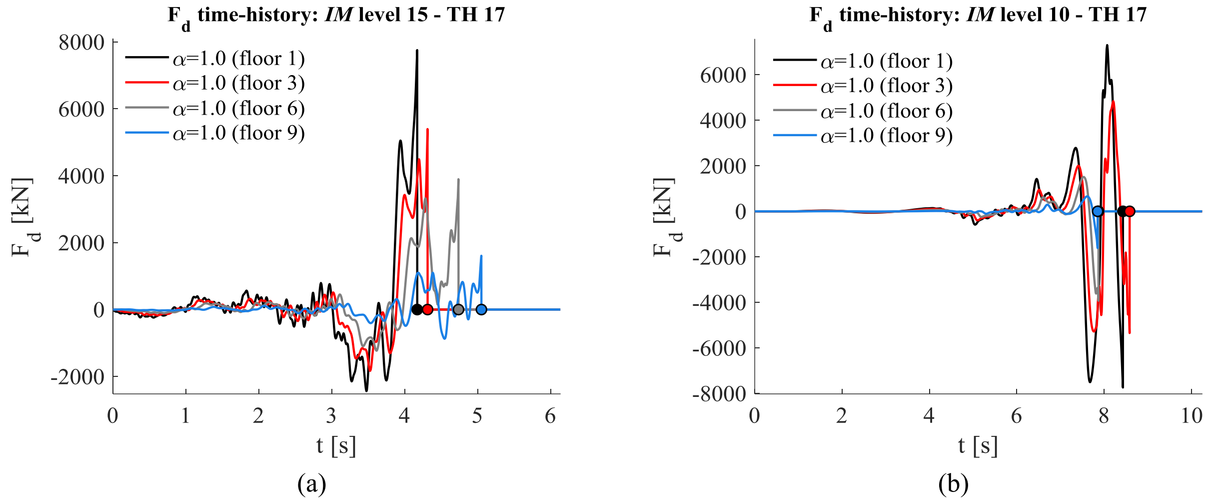

Fig. 11. Failure time-lag among dampers at different floors: *IM* level n. 15 (a) and 10 (b) *IM*.

4.3 *Qualitative evaluation of the overall probabilistic response*

In this section a preliminary evaluation of the overall probabilistic response of the three-storey building is provided. **Fig. 12** shows the building response in terms of IDR and acceleration at storeys (A) at different seismic intensities for the case of linear dampers ($\alpha = 1.0$). For each *IM* level, the median response values are shown by using continuous lines with circle markers, and different colours are used to compare the following three cases: 1) bare model (black); 2) building with dampers designed without amplification factors ($\gamma_v = \gamma_\Delta = 1$) (blue); 3) building with dampers with neither impact nor failure model ($\gamma_v = \gamma_\Delta = \infty$) (red). Moreover, the 16th and 84th percentiles are plotted by dotted lines by using the same colours described above.

The following observations can be made:

- FVDs without failure significantly reduce the IDR of the building up to the highest seismic intensities, with a lower beneficial effect in terms of acceleration mitigation;
- If the device failure is taken into account, the response mitigation provided by the dampers vanishes for *IM* levels higher than 10, corresponding to design condition (0.8866 *g*);
- Once failed, devices are no longer effective and the IDR response of the damped systems tends to be almost that of the bare building, while the response in acceleration shows peaks higher than the undamped frame system, due to the impacts induced by the devices end-stroke attainment.

The observations above also apply to the case with nonlinear dampers (not shown due to space constraints).

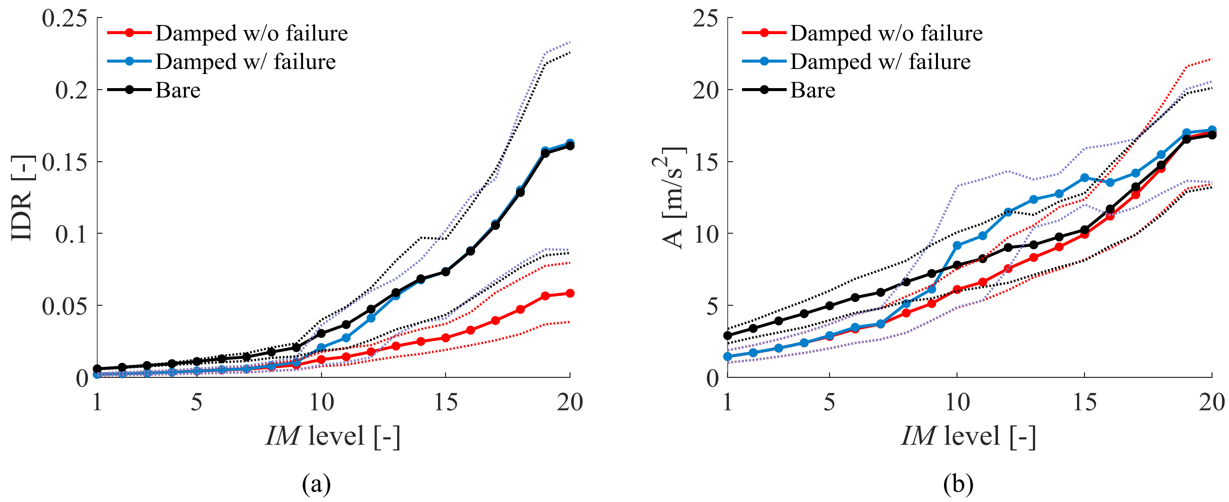

Fig. 12. Building response at different *IM* levels for the case with linear dampers (α=1.0) in terms of (a) IDR and (b) A. Comparison between damped (with and without failure) and bare model.

5 PROBABILISTIC ANALYSIS RESULTS: THREE-STOREY BUILDING

The performance of the case studies is evaluated by monitoring a wide set of EDPs. To provide information on the damage level of the main structural system, the following global EDPs are considered: the maximum interstorey drift among the various storeys (IDR), the maximum roof drift (RDR), the maximum residual interstorey drift among the storeys (IDR_{res}), and the maximum absolute acceleration at storeys (A). The dampers performance is monitored by considering the following two local EDPs, accounting for the cost, the size and the failure of the devices: the maximum absolute force of the dampers (F_{di}) and the maximum stroke (Δ_{di}).

5.1 Demand hazard curves

This subsection shows the demand hazard curves of all the monitored EDPs, with respect to the mean annual rate of exceedance ν_D, for each damper typology ($\alpha = 1.0, \alpha = 0.6, \alpha = 0.3$). Comparisons are made among the various analysed cases, namely: dampers without amplification factors ($\gamma_v = \gamma_\Delta = 1.0$) (blue solid line) and dampers designed with different γ factors, that is $\gamma_v = 1.5$ and $\gamma_\Delta = 1.0$ (brown solid line); $\gamma_v = \gamma_\Delta = 1.5$ (yellow solid line); $\gamma_v = \gamma_\Delta = 2.0$ (violet solid line); $\gamma_v = \gamma_\Delta = 3.0$ (green solid line). Moreover, the demand hazard curve of the following two cases are added for comparison purposes: bare frame model (black dashed line) and damped model without damper failure (i.e., with $\gamma_\Delta = \gamma_v = \infty$) (red solid line). Also, two horizontal dotted lines are depicted in the charts, one identifying the design hazard level 0.0021 yr^{-1} (black dotted line) and the other (red dotted line) denoting the target risk level desired for the structural systems ($2x10^{-4}$ yr^{-1}) [23][24].

Results concerning the linearly damped building are first presented. The demand hazard curves of the main global EDPs (IDR, RDR, IDR_{res}, A) are illustrated in **Fig. 13**, whereas those concerning the damper response (F_{di} and Δ_{di}) are illustrated in **Fig. 16**. Only the curves of the dampers at floor 1 are shown, given the similarity of the results among the storeys.

Based on **Fig. 13** the following comments can be made:

- For all the cases with dampers and amplification factors larger than 1.0, the rate of exceeding of the target drift performance (IDR=0.012) is around 0.0021 yr^{-1}, the hazard level of the design action, represented by the horizontal black dotted line, with some slight deviations that can be justified by the probabilistic nature of the analysis (contribution to the exceedance probability from *IM* levels different from the reference one [29][30]).
- If no amplification is considered ($\gamma_v = \gamma_\Delta = 1$, blue curve), the rate of exceeding of the target drift performance, highlighted by the red dotted line (IDR=0.012), is notably higher than the expected one, due to the failures experienced by the dampers at intensity levels lower than the design one (i.e., *IM* = 0.89 *g*) (see Section 5.3 for further details about this point).
- Once damper rupture is attained, the building response in terms of maximum and residual drift tends to that of the bare model (black dashed line) and the magnitude of the amplification factors governs the "rapidity" of the transition from the damped to the bare frame curve.
- In particular, the IDR, RDR and IDR_{res} approach the bare frame model quite perfectly, conversely, the absolute accelerations, which are lower than those of the bare frame until the dampers are effective, become even higher due to end-strokes impacts experienced by the dampers, before their failures.
- The hazard curves of RDR and IDR are very similar and both of them tend to overlap those of the bare model once the dampers fail, meaning that, in this case, the drift demand is uniform along the building height (no soft storey mechanisms have been observed).

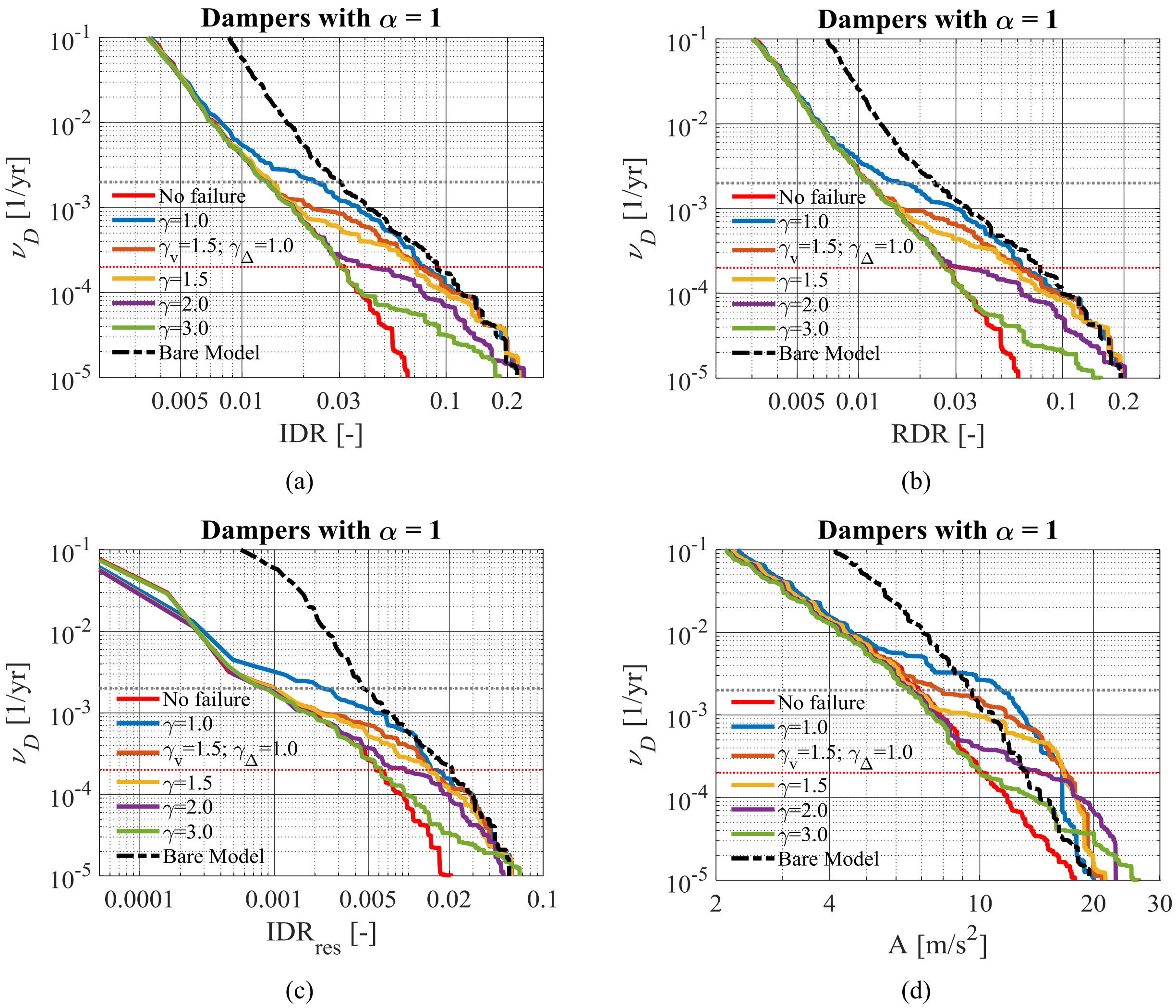

Fig. 13. Demand hazard curves of the main global EDPs (a) IDR, (b) RDR, (c) IDR_{res}, (d) A for different damper amplification factors. Case of building with linear dampers ($\alpha = 1.0$).

Fig. 14 shows the IDR demand hazard curves for the cases with nonlinear dampers (α=0.6 and α=0.3). The trends are similar to those observed with linear dampers, although there are some differences worth to be stressed:

- The curves of nonlinear dampers have a lower slope, which lead the system to show, for a given demand value, higher exceedance annual rates. This is consistent with previous studies comparing the performance of linear and nonlinear FVDs [29].
- The MAF levels corresponding to the transition from the curve of the damped system to that of the undamped one are higher for nonlinear dampers compared to the linear ones, and the slope of such transition increases with the degree of nonlinearity of dampers.

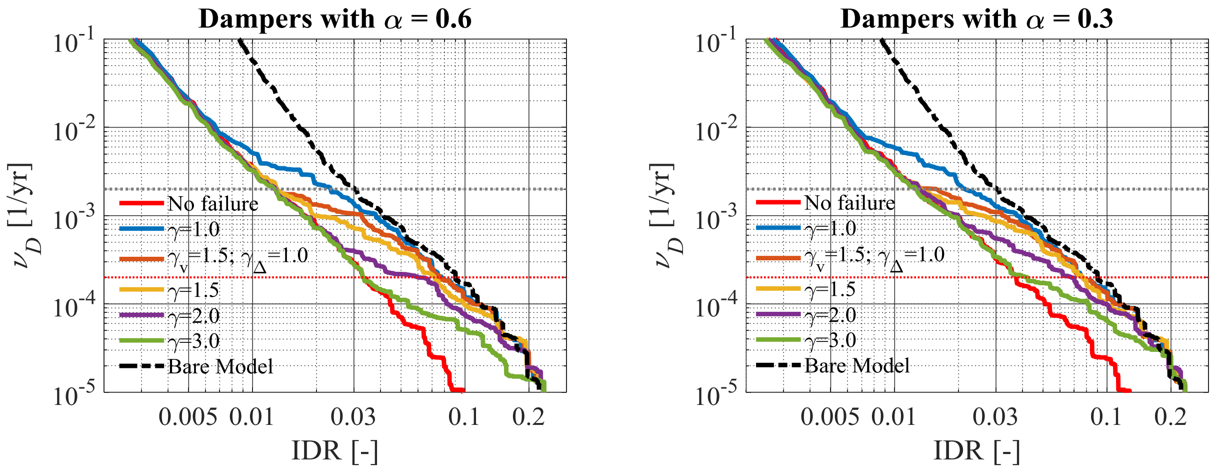

(a) (b)

Fig. 14. Demand hazard curves of the IDR parameter for different damper's amplification factors. Case of building with nonlinear dampers: (a) α=0.6; (b) α=0.3.

Finally, a deeper discussion is due on the influence of the amplification factors on the structure reliability (**Fig. 15**). For this purpose, the response corresponding to the reference MAF of 2x10^{-4} is selected. This value is generally considered as a satisfactory target for the MAF of collapse, as illustrated in [23][54]. The response corresponding to the reference MAF, in terms of IDR, achieved for the case where no damper failure is permitted ("No Failure") is assumed as the target response and identified as IDR_0. This result is then compared, through the ratio IDR/IDR_0, with the values of IDR achieved with four different values of the γ-factors. The analysed cases are $\gamma_v = \gamma_\Delta = 1.0$, that is dampers without amplification factors and three more cases in which the displacements and the forces associated with velocities are amplified, that is $\gamma_v = \gamma_\Delta = 1.5$, $\gamma_v = \gamma_\Delta = 2.0$ and $\gamma_v = \gamma_\Delta = 3.0$.

Fig. 15 shows the variation with γ of the ratio IDR/IDR_0 highlighting that in the case of linear dampers, the use of a γ-factor equal to 3 permits to obtain the same IDR of the "No failure" case, whereas in the case of nonlinear devices a value just larger than 1 is reached, ensuring similar performance in both the linear and nonlinear case. Differently, with lower values of γ-factors, significantly larger values of the ratio IDR/IDR_0 are obtained, meaning that the response achieved when accounting for the devices failure is far from the reference one (IDR_0). The trend of the ratio achieved with linear dampers seems to be more sensible to the variation of the γ-factors, as highlighted by a change of the slope when γ are comprised between 1.5 and 2. Differently, with nonlinear devices the trend has a slighter slope, highlighting a value of the ratio IDR/IDR_0 closer to 1 for higher values of the γ-factors.

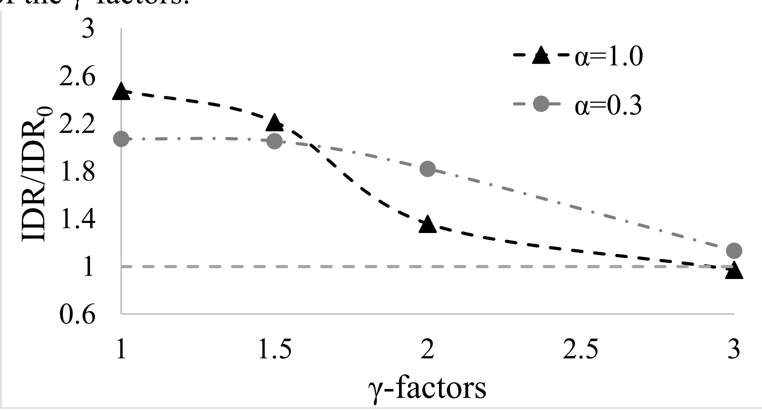

Fig. 15. Ratios IDR/IDR_0 for different damper amplification factors. Case of building with linear dampers ($\alpha = 1.0$) and nonlinear dampers ($\alpha = 0.3$).

5.2 Dampers failure rates

This sub-section examines the demand hazard curves of the EDPs related to the dampers, i.e., the maximum force and the maximum stroke. **Fig. 16** illustrates the curves of the maximum force (**Fig. 16**a) and the maximum stroke (**Fig. 16**b) for the linear damper ($\alpha = 1.0$) at floor n. 1. These are representative of the outcomes observed at all the floors and the trends observed are the same for all the types of dampers ($\alpha = 0.6, \alpha = 0.3$). Some general comments on **Fig. 16** follow, which also apply to all the other cases not displayed in the plots:

- Dampers designed with $\gamma_v = \gamma_\Delta = 1.0$ (blue curves) fail at a MAF of exceedance higher than the design hazard level 0.0021 yr^{-1} (black dotted lines), mainly because of over-velocity phenomena which lead the dampers to attain the ultimate force capacity.
- Despite the ultimate force capacity is the same, the annual rate of failure for the case $\gamma_v = 1.5$ and $\gamma_\Delta = 1.0$ (brown curves) is higher than the case $\gamma_v = \gamma_\Delta = 1.5$ (yellow curves) due to the higher number of collapses induced by the end-stroke attainment.
- All the curves follow the trend of the case with dampers with unlimited capacity (red curves) until the collapse is attained, then the curves show a sudden vertical drop due to the impossibility to exceed the ultimate capacity values.

Table 7 to **Table 9** summarise the damper failure rates (ν_{fail}) for all the cases analysed, by also providing the values of ν_{fail}/ν_{target}, i.e., the ratios between the actual failure rates and the target risk levels desired for the structural systems ($2x10^{-4}$ yr^{-1}) [23]. Ratios higher than one identify cases in which the target reliability level is not attained, ratios equal or lower than one identify cases in which the requirement is fulfilled (such values are highlighted by bold font in the tables). It can be observed that without amplification factors the failure is always attained with a probability higher than the target one. If the amplification factors are used, the higher the amplification factors, the lower the ν_{fail}/ν_{target} ratios are. When the amplification factor $\gamma_v = \gamma_\Delta = 3.0$ is applied, the ratios are always lower than one, except for the nonlinear dampers with $\alpha = 0.3$ at the first and last elevation.

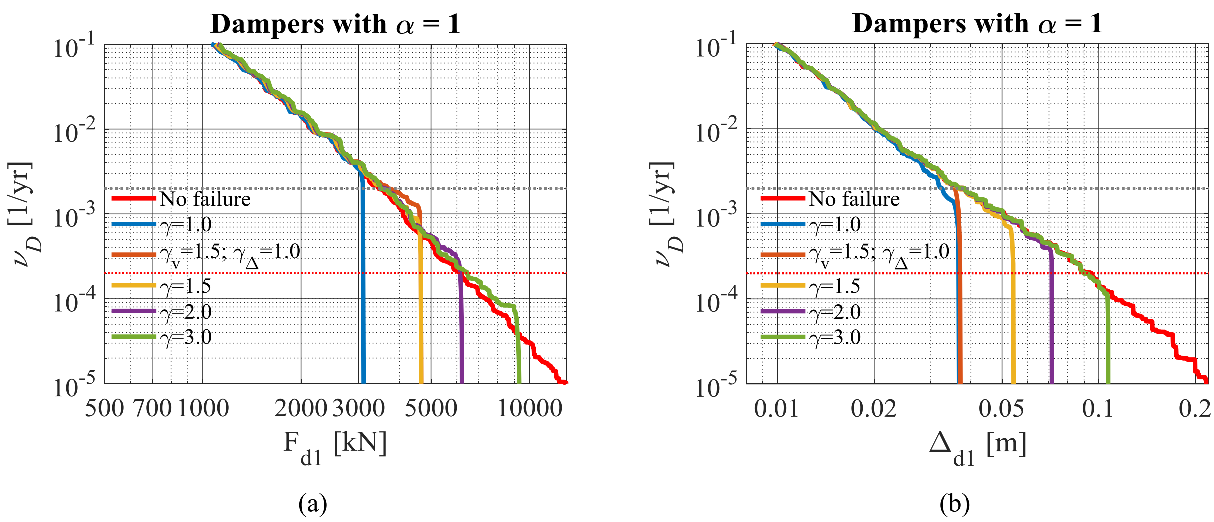

Fig. 16. Demand hazard curves of the main local EDPs (a) dampers force F_{di} and (b) stroke Δ_{di} for different damper amplification factors. Case of building with linear dampers ($\alpha = 1.0$).

Table 7. Damper failure rates (ν_{fail}) and ν_{fail}/ν_{target} ratios of the 3-storey building ($\alpha = 1.0$).

Case of analysis	ν_{fail} [1/yr]			ν_{fail}/ν_{target} [-]		
	Floor 1	Floor 2	Floor 3	Floor 1	Floor 2	Floor 3
$\gamma_\Delta = \gamma_v = 1.0$	3.48E-03	3.93E-03	5.45E-03	17.42	19.65	27.26
$\gamma_\Delta = 1.0$ & $\gamma_v = 1.5$	1.28E-03	1.21E-03	1.54E-03	6.38	6.05	7.70
$\gamma_\Delta = \gamma_v = 1.5$	8.80E-04	7.43E-04	1.01E-03	4.40	3.72	5.05
$\gamma_\Delta = \gamma_v = 2.0$	2.99E-04	2.57E-04	2.41E-04	1.50	1.29	1.20
$\gamma_\Delta = \gamma_v = 3.0$	8.20E-05	3.53E-05	5.41E-05	**0.41**	**0.18**	**0.27**

Table 8. Damper failure rates (ν_{fail}) and ν_{fail}/ν_{target} ratios of the 3-storey building ($\alpha = 0.6$).

Case of analysis	ν_{fail} [1/yr]			ν_{fail}/ν_{target} [-]		
	Floor 1	Floor 2	Floor 3	Floor 1	Floor 2	Floor 3
$\gamma_\Delta = \gamma_v = 1.0$	4.08E-03	3.69E-03	4.97E-03	20.39	18.44	24.87
$\gamma_\Delta = 1.0$ & $\gamma_v = 1.5$	1.68E-03	1.89E-03	1.71E-03	8.38	9.45	8.55
$\gamma_\Delta = \gamma_v = 1.5$	1.26E-03	1.33E-03	1.16E-03	6.30	6.65	5.82
$\gamma_\Delta = \gamma_v = 2.0$	4.42E-04	4.46E-04	4.28E-04	2.21	2.23	2.14
$\gamma_\Delta = \gamma_v = 3.0$	1.54E-04	1.33E-04	1.32E-04	**0.77**	**0.66**	**0.66**

Table 9. Damper failure rates (ν_{fail}) and ν_{fail}/ν_{target} ratios of the 3-storey building ($\alpha = 0.3$).

Case of analysis	ν_{fail} [1/yr]			ν_{fail}/ν_{target} [-]		
	Floor 1	Floor 2	Floor 3	Floor 1	Floor 2	Floor 3
$\gamma_\Delta = \gamma_v = 1.0$	4.86E-03	5.21E-03	7.72E-03	24.30	26.07	38.59
$\gamma_\Delta = 1.0$ & $\gamma_v = 1.5$	2.06E-03	2.04E-03	2.50E-03	10.60	10.22	12.49
$\gamma_\Delta = \gamma_v = 1.5$	1.61E-03	1.60E-03	1.94E-03	8.07	8.02	9.70
$\gamma_\Delta = \gamma_v = 2.0$	6.27E-04	7.58E-04	8.24E-04	3.14	3.79	4.12
$\gamma_\Delta = \gamma_v = 3.0$	2.48E-04	1.81E-04	2.25E-04	1.24	**0.91**	1.12

Finally, further light is shed regarding the effect of the amplification factors on the sequence of dampers failure among different storeys. For this purpose, it can be useful to refer to **Fig. 17**, where the average trends of the $F_d/F_{d,max}$ ratios are depicted (together with the 16th and 84th response percentiles), for different intensity levels and for all the building storeys. Being all the curves almost perfectly overlapped, it means that there are not cases in which some devices remain active while others fail. The only exception to this general result is represented by the case in which high γ-factors ($\gamma_v = \gamma_\Delta = 3$) are used. Indeed, beside the curve shifting towards higher *IM*s, curves of dampers belonging to different floors slightly deviate at the highest seismic intensities, by testifying the presence of few cases in which the dampers at the higher floors do not fail together with the other located at the lower floors. This aspect will be further discussed for the case of the 9-strey building, which shows a higher sensitivity to the γ-factor values. The results obtained for nonlinear dampers are similar to the ones presented here and are not reported due to space constraints.

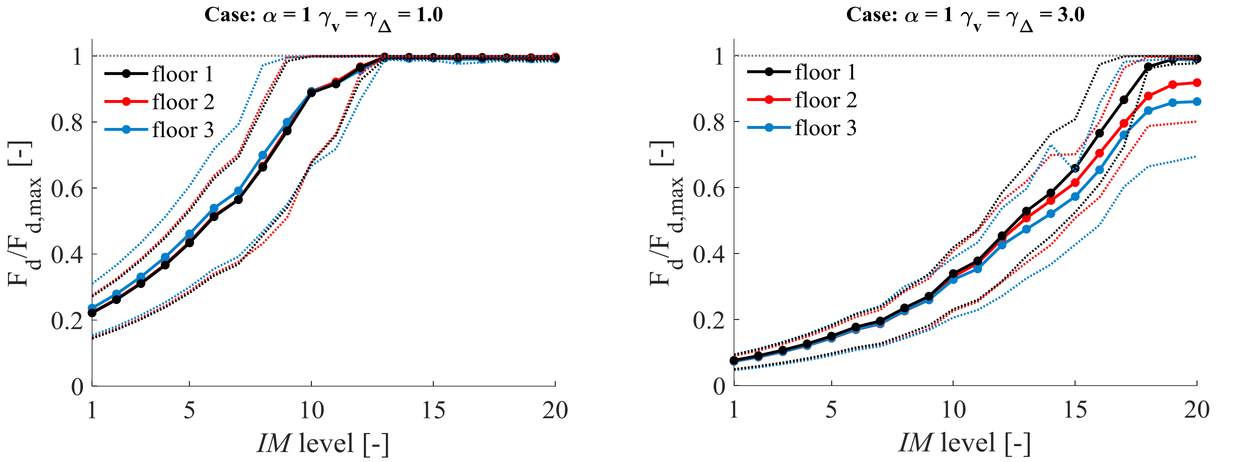

(a) (b)

Fig. 17. Average and 16th and 84th response percentiles of the $F_d/F_{d,max}$ – IM trends at different floors for γ factors (a) $\gamma_v = \gamma_\Delta = 1$ and (b) $\gamma_v = \gamma_\Delta = 3$.

5.3 Dampers collapse fragility functions

In this section, the problem of damper failure is analysed in terms of fragility functions $\mathrm{G_{fail|IM}}$, providing information about the dependency of the probability of failure with the seismic intensity. **Fig. 18** shows the fragility curves of the linear dampers placed at the first and third floor, for all the different γ-factors analysed.

Based on these results, the following observations can be made:

- The absence of amplification factors leads to high damper failure probabilities (>50%) at seismic intensities lower than the design level (i.e., *IM* = 0.89 *g*), and from *IM* = 1.5 *g* a 100% probability of damper failure is obtained.
- The beneficial effect of γ-factors larger than 1 is testified by the shifting of the fragility curves towards higher seismic intensities.
- Failure probabilities also reduce by moving from floor 1 to floor 3, as can be observed by comparing the curve of **Fig. 18**a and **Fig. 18**b. However, no differences are observed among the floors for the case without amplification ($\gamma_v = \gamma_\Delta = 1$).

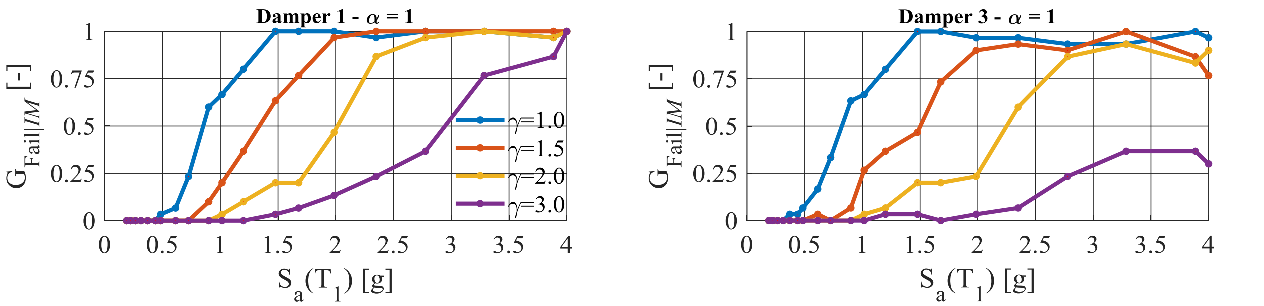

(a) (b)

Fig. 18. Damper collapse fragility at (a) floor 1 and (b) floor 3 with different amplification factors. Case of building with linear dampers ($\alpha = 1.0$).

Comments above also apply to the case with nonlinear dampers ($\alpha = 0.3$, shown in **Fig. 19**), with the main exception given by the slightly higher failure probabilities observed in this latter case.

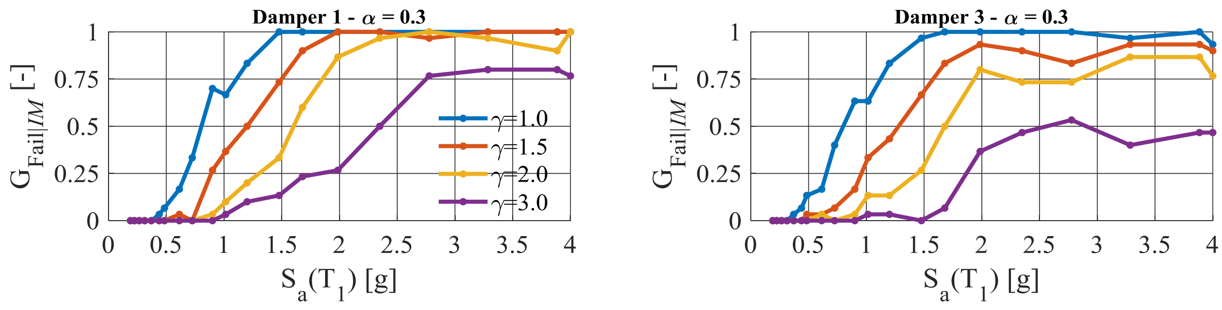

(a) (b)

Fig. 19. Damper collapse fragility at (a) floor n. 1 and (b) floor 3 with different amplification factors. Case of building with nonlinear dampers (α=0.3).

6 PROBABILISTIC ANALYSIS RESULTS: NINE-STOREY BUILDING

This section shows the results concerning the 9-storey building. Due to space constraints, only selected results are presented. The differences between the seismic response of this structural system and the previous low-rise building are highlighted, with particular focus on the effect of the amplification factors on the sequence of dampers failure along the storeys, and the levels of seismic reliability that are achieved.

6.1 Demand hazard curves and failure probabilities

Fig. 20 and **Fig. 21** show the demand hazard curves of the 9-storey building equipped respectively with linear and nonlinear dampers. In general, the curves follow the same trends observed for the low-rise system. However, in this case the MAF levels at which the curves start diverging due to damper failure are notably higher. For instance, the case without amplification factors (blue curve) deviates from the "no failure" case (red curve) at $\nu = 10^{-2}$ yr^{-1}. This is due to the fact that the damper design is carried out based on the first mode response approximation, which is less accurate for the medium and high-rise buildings, whose response is significantly influenced by higher-order modes.

Moreover, by comparing **Fig. 20** a) and **Fig. 21** a) it is worth noting that the efficiency of the added dampers reduces for decreasing MAF of exceedances. In fact, higher reductions of drifts are observed for higher MAF of exceedances than for lower ones, for both the cases of linear and nonlinear dampers. In this regard, the nonlinear behaviour of the frame (and consequent period-elongation) has a significant contribution and affects the dampers performance and their efficiency. It is also observed that the beneficial effect in terms of IDR reduction reduces for increasing levels of nonlinearity of the dampers (i.e. lower alpha values). In fact, as already highlighted in previous works carried out by the authors ([29]-[31]), the nonlinear devices are more effective with respect to the linear ones in controlling the viscous forces, while this efficiency is paid in terms of higher displacements, particularly for less probable events (lower MAF of exceedance).

The use of amplification factors improves the response by shifting the curves towards lower failure probabilities, as already shown previously for the low-rise building. However, results are worse in terms of system reliability levels achieved with respect to the 3-stroey building.

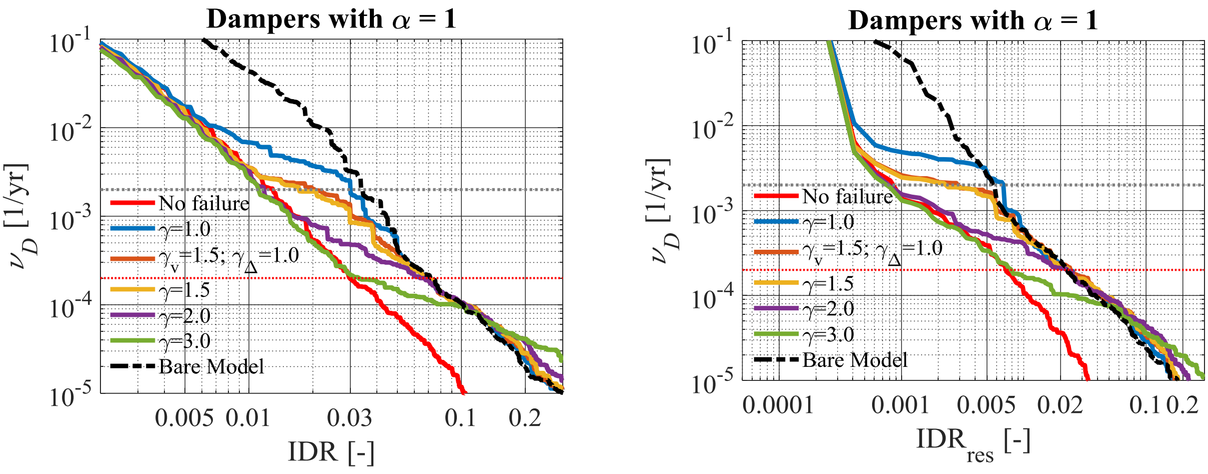

(a) (b)

Fig. 20. Demand hazard curves of the main global EDPs (a) IDR, (b) IDR_{res} for different damper amplification factors. Case of building with linear dampers ($\alpha = 1.0$).

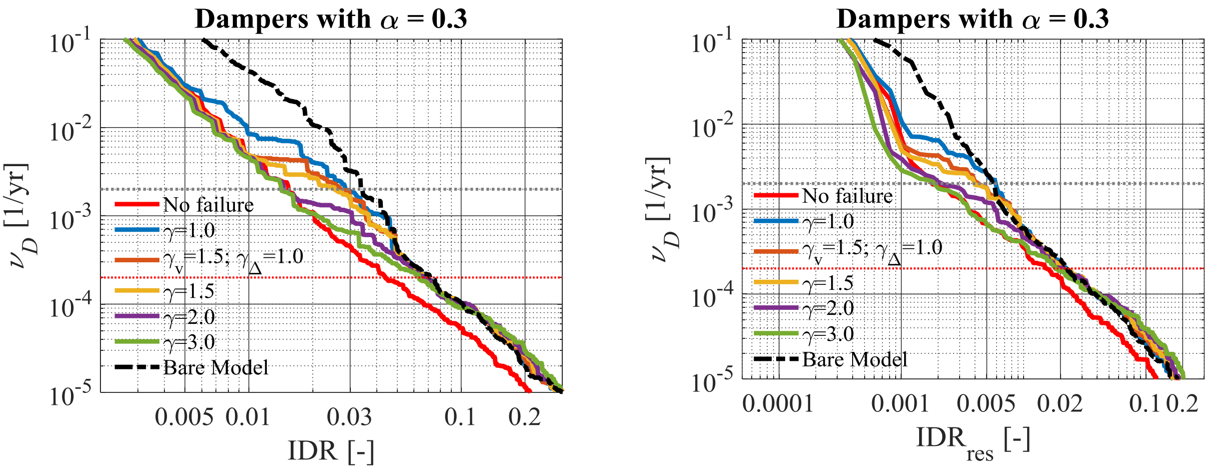

(a) (b)

Fig. 21. Demand hazard curves of the main global EDPs (a) IDR, (b) IDR_{res} for different damper amplification factors. Case of building with nonlinear dampers ($\alpha = 0.3$).

As already done for the 3-storey building, with the aim to provide an insight on the influence of the response amplification factors on the damper failure probability, the IDR response corresponding to the target MAF of exceedance of $2x10^{-4}$ is evaluated for different values of γ-factors, and normalized with respect to the response obtained with dampers that do not suffer failure (IDR_0). **Fig. 22** shows the results obtained with γ-factors ranging from 1 to 3 for linear devices (α=1.0) and nonlinear ones (α=0.3). It can be observed that, differently from the 3-storey building, the trends obtained with linear and nonlinear devices are significantly different among them. With linear dampers, indeed, the use of γ-factors equals to 3 leads nearly to the achievement of the desired response (IDR_0), ensuring a ratio IDR/IDR_0 slightly higher than one, while lower values of γ-factors correspond to higher values of the ratio. Differently, the response achieved with nonlinear dampers seems to be insensitive to change of the γ-factors, with a ratio IDR/IDR_0 that always remains comprised between 1.56 and 1.43.

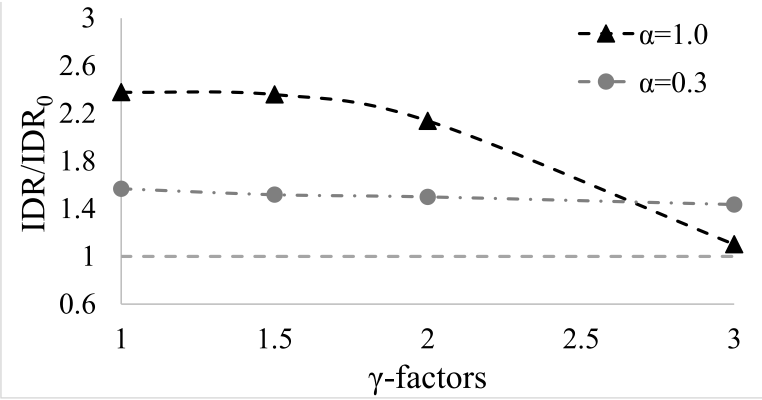

Fig. 22. Ratios IDR/IDR0 for different damper's amplification factors. Case of building with linear dampers ($\alpha = 1.0$) and nonlinear dampers ($\alpha = 0.3$).

Regarding the effect of the amplification factors on the sequence of dampers failure, some further details are provided in **Fig. 23**, as already done for the 3-storey building. In general, it is observed that when one device fails, all the other devices fail too, even though at different times. However, this not always true, and in order to analyse this issue it can be useful to refer to **Fig. 23**, where the average trends of the $F_d/F_{d,max}$ ratios are depicted, for different intensity levels and for different building storeys (i.e., floors n. 1, 3, 6, 9). When no amplification factors are used ($\gamma_v = \gamma_\Delta = 1$), the curves are almost perfectly overlapped (**Fig. 23** a), thus there are not cases in which some devices remain active while others fail. The response changes if higher γ-factors are used, as shown in **Fig. 23** b ($\gamma_v = \gamma_\Delta = 3$). Indeed, beside the curve shifting towards higher *IM*s, curves of dampers belonging to the upper floors slightly deviate at the highest seismic intensities, by testifying a lower average rate of failures, and thus a concentration of collapse cases in the dampers at the lower floors. It is noteworthy that the damage concentration on the structural elements at the storeys with failed (inactive) dampers results in a building performance worse than the one of the bare frame case, this result can be also related to the design method used for the FVDs, which disregards higher order modes.

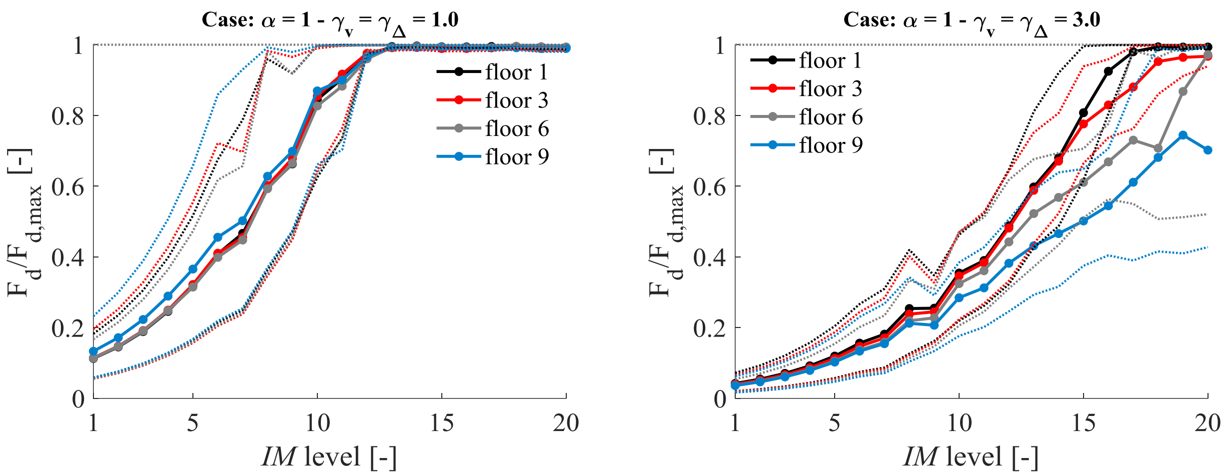

(a) (b)

Fig. 23. Average and 16th and 84th response percentiles of the $F_d/F_{d,max}$ – IM trends at different floors for linear dampers with (a) $\gamma_v = \gamma_\Delta = 1$ and (b) $\gamma_v = \gamma_\Delta = 3$.

The damper reliability is also analysed by showing in **Fig. 24** and **Fig. 25** the fragility functions for, respectively, the linear and nonlinear dampers placed at different floors, for the different γ-factors analysed. The results shown in these figures are very similar to those obtained for the 3-floors building (**Fig. 18** and **Fig. 19**). However, in this case the differences between the fragilities of dampers placed at different floors is more evident, thus confirming that a more specialized design method for the FVDs or different amplification factors at different floors should be used in order to obtain a uniform failure among dampers of different storeys, as already observed previously.

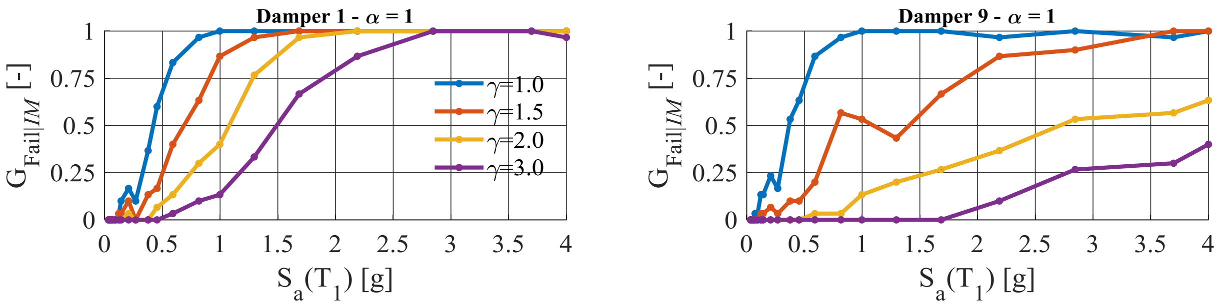

(a) (b)

Fig. 24. Damper collapse fragility at (a) floor 1 and (b) 9, with and withouth amplification factors. Case of building with linear dampers ($\alpha = 1.0$).

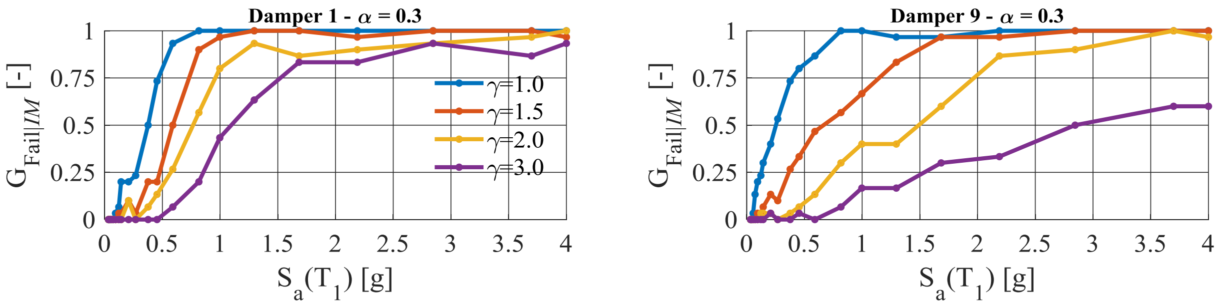

(a) (b)

Fig. 25. Damper collapse fragility at (a) floor 1 and (b) 9, with and withouth amplification factors. Case of building with nonlinear dampers ($\alpha = 0.3$).

7 CONCLUSIONS

The seismic design of Fluid Viscous Dampers (FVDs) for enhancing the performance of buildings should ensure proper safety margins against their collapse, and the reliability of the whole structural system is strongly influenced by the reliability of these devices. Seismic standards generally prescribe that that the FVDs must be designed based on values of the response parameters (i.e., stroke and velocity) evaluated at the design condition and amplified by safety factors (reliability factors), in order to reach a target level of safety. However, the values of these reliability factors are not homogenous among the various codes and the level of safety attainable through their use has not been sufficiently investigated.

The present paper investigates the issue through the analysis of two benchmark case studies consisting of a low-rise and a medium-rise steel building equipped with FVDs. A wide range of safety factor values is considered for the damper design, considering suggestions from international seismic codes (EN15129 and ASCE-41). A wide parametric investigation is carried out to explore the influence of these safety factors on both the fragility and the seismic risk of the whole structural system. The effect of damper nonlinearity is also taken into account analysing damper velocity exponents ranging from 0.3 to 1.0. The damper shows a brittle failure when its internal force attains the device strength and this may occur for two reasons: impact when end-stroke is attained, or attainment of excessive velocity. Both these failure modalities are described by the structural model and considered in the analyses.

As a general result, it is observed that combined effects of impacts and extreme velocities may induce a global brittle behaviour that cannot be perceived by models neglecting these phenomena. More specifically, based on the outcomes of the present study, the following conclusions can be drawn:

- The consequences of the damper failure on the performance of the whole structural system depend on the number of dampers remained active: if all dampers fail together, then the system response tends to that of the bare building, however absolute accelerations may be higher as a consequence of impacts and dissipation concentrated at some storeys only may leads to a worse global response.
- The likelihood of the damper failure as well as the "rapidity" of the response transition from damped to bare (or partially damped) structural system are governed by the magnitude of the two amplification factors ($\gamma_{\Delta}, \gamma_{v}$) adopted for damper stroke and velocity.
- If no amplification is provided ($\gamma_v = \gamma_\Delta = 1.0$), the dampers probability of failure is higher than the design hazard level (assumed equal to 0.0021 yr^{-1} in this work), thus, dampers experience failure at intensity levels lower than the design one.
- The use of amplification factors higher than 1.0 allows attaining lower failure probabilities, and this beneficial effect is more significant for larger γ–factors.
- Nonlinear dampers (α=0.3) exhibit higher failure probabilities (about two times) than the linear ones; moreover, the transition from the damped response (active devices) to that of the undamped one (failed devices) increases at a faster rate increasing the degree of damper nonlinearity.
- In tall buildings where a design method disregarding higher order modes is used for FVDs, non-uniform failures among dampers of different storeys may occur.

Based on the study results, some suggestions can be proposed for further improvements of the design prescriptions of the main international seismic codes. First of all, it should be observed that γ–factors equal to 3, both for stroke and velocity, generally ensure that the target failure probability $2x10^{-4}$ yr^{-1} is achieved, despite they might result inadequate in case of dampers with strong nonlinear behaviour (i.e., α = 0.3 or lower). Such result, also observed in the 9-storey building, confirms the need of extending the study to γ-factors higher than 3.0. Additionally, the study outcomes suggest that in the case of medium and high-rise buildings, different γ-factors should be employed at the various storeys, and they should be tailored to the specific damper properties present at each storey. It might be also worth to investigate the problem of γ-factors by analysing more closely the damage/plasticity evolution and distribution over the structural elements when devices fail. Moreover, it should be observed that the choice of γ–factors depends on the ratio between the MAF of exceedance chosen for the seismic design action and the target MAF of failure. For example, ASCE code suggests lower MAF for seismic design actions and relevant γ–factors seem to be in line with suggested target value of MAF of failure.

It is also worth to note that the amplification of the damper velocity only, without a corresponding amplification of the damper stroke (i.e., $\gamma_\Delta = 1.0$ and $\gamma_v > 1.0$), as allowed by the European code EN15129, does not provide significant beneficial effects because the impacts due to the end-stroke attainment makes the effect of γ_v useless. Thus, homogeneous amplification factors (i.e., $\gamma_\Delta = \gamma_v$) should be used to achieve a reliable and effective design of FVDs.

Given the relevance of these aspects, the extension of the study to a wider range of buildings typologies and design methods will be considered in future works.

REFERENCES

[1] Tubaldi, E., Gioiella, L., Scozzese, F., Ragni, L., & Dall'Asta, A. (2020). A design method for viscous dampers connecting adjacent structures. *Frontiers in Built Environment*, *6*, 25.

[2] Barroso LR. Performance evaluation of vibration controlled steel structures under seismic loads. PhD thesis, Stanford University, California, US, 1999.

[3] Pavlou, E, Constantinou, M.C., 2006. Response of Nonstructural Components in Structures with Damping Systems, *Journal of Structural Engineering*, **132**(7), 1108-1117.

[4] Lavan, O, Dargush, G.F., 2009. Multi-Objective Evolutionary Seismic Design with Passive Energy Dissipation Systems, *Journal of Earthquake Engineering*, **13**(6), 758-790.

[5] Gioiella, L., Tubaldi, E., Gara, F., Dezi, L., Dall'Asta, A. (2018). Modal properties and seismic behaviour of buildings equipped with external dissipative pinned rocking braced frames. *Engineering Structures, 172*. https://doi.org/10.1016/j.engstruct.2018.06.043

[6] Pavia, A., Scozzese, F., Petrucci, E., & Zona, A. (2021). Seismic Upgrading of a Historical Masonry Bell Tower through an Internal Dissipative Steel Structure. Buildings, 11(1), 24.

[7] Gioiella, L., Tubaldi, E., Gara, F., Dezi, L., Dall'Asta, A. (2018). Stochastic Seismic Analysis and Comparison of Alternative External Dissipative Systems. *Shock and Vibrations, 47*. https://doi.org/10.1155/2018/5403737

[8] Tubaldi, E. (2015). Dynamic behavior of adjacent buildings connected by linear viscous/viscoelastic dampers. *Structural Control and Health Monitoring*, **22**(8), 1086-1102.

[9] Hwang, JS., Lin, WC., Wu, NJ. (2010). Comparison of distribution methods for viscous damping coefficients to building. *Structure and Infrastructure Engineering: Maintenance, Management, Life-Cycle Design and Performance, 9*(1), 28-41. http://dx.doi.org/10.1080/15732479.2010.513713

[10] Silvestri, S., Palermo, M., & Trombetti, T. (2018). A direct procedure for the seismic design of frame structures with added viscous dampers. *Seismic Resistant Structures*, 37.

[11] Tubaldi, E., Barbato, M., Dall'Asta, A., 2015. Efficient approach for the reliability-based design of linear damping devices for seismic protection of buildings. ASCE-ASME Journal of Risk and Uncertainty in Engineering Systems, Part A: Civil Engineering, 2(2), C4015009. DOI: 10.1061/AJRUA6.0000858.

[12] Palermo, M., Silvestri, S., Landi, L., Gasparini, G., & Trombetti, T. (2018). A "direct five-step procedure" for the preliminary seismic design of buildings with added viscous dampers. *Engineering Structures*, *173*, 933-950.

[13] Altieri, D., Tubaldi, E., De Angelis, M., Patelli, E., & Dall'Asta, A. (2018). Reliability-based optimal design of nonlinear viscous dampers for the seismic protection of structural systems. *Bulletin of Earthquake Engineering*, *16*(2), 963-982.

[14] Pollini, N., Lavan, O., & Amir, O. (2018). Optimization- based minimum- cost seismic retrofitting of hysteretic frames with nonlinear fluid viscous dampers. *Earthquake Engineering & Structural Dynamics*, *47*(15), 2985-3005.

[15] De Domenico, D., Ricciardi, G., & Takewaki, I. (2019). Design strategies of viscous dampers for seismic protection of building structures: a review. *Soil Dynamics and Earthquake Engineering*, *118*, 144-165.

[16] Victorsson, V.K. (2011). The reliability of capacity-designed components in seismic resistant systems. *PhD thesis*, Stanford University, California, US.

[17] Tirca, L. and Chen, L. (2014). Numerical simulation of inelastic cyclic response of HSS braces upon fracture. *Advanced Steel Construction,* 10(**4**), 442-462.

[18] Matsui, R., Takeuchi, T., Urui, S., & Tokuno, M. (2018). Collapse Analysis of Steel Frames Considering Fracture of Braces and End of Beams. In Key Engineering Materials (Vol. 763, pp. 686-693). Trans Tech Publications.

[19] American Society of Civil Engineers. Seismic Evaluation and Retrofit of Existing Buildings: ASCE Standard ASCE/SEI 41-17. American Society of Civil Engineers, 2017.

[20] European Committee for Standardization. EN 15129:2010 - Antiseismic devices, Brussels, Belgium, 2010

[21] European Committee for Standardization. Eurocode 8-Design of Structures for Earthquake Resistance. Part 1: General Rules, Seismic Actions and Rules for Buildings, Brussels, Belgium, 2004.

[22] ASCE (American Society of Civil Engineers). (2010). Minimum design loads for buildings and other structures. *Standard ASCE/SEI 7-10*.

[23] Fajfar, P. (2018). Analysis in seismic provisions for buildings: past, present and future. *Bulletin of Earthquake Engineering*, **16**, 2567-2608. DOI:°10.1007/s10518-017-0290-8

[24] Gkimprixis, A., Tubaldi, E., & Douglas, J. (2019). Comparison of methods to develop risk-targeted seismic design maps. *Bulletin of earthquake engineering,* 17(7), 3727-3752.

[25] Seo, C.Y., Karavasilis, T.L., Ricles, J.M, Sause, R., 2014. Seismic performance and probabilistic collapse resistance assessment of steel moment resisting frames with fluid viscous dampers, Earthquake Engineering and Structural Dynamics, 43(14), 2135-2154.

[26] Gidaris, I., Taflanidis, A.A., 2015. Performance assessment and optimization of fluid viscous dampers through life-cycle cost criteria and comparison to alternative design approaches. Bulletin of Earthquake Engineering, 13, 1003-1028.

[27] Tubaldi, E., Barbato, M., Dall'Asta, A., 2014. Performance-based seismic risk assessment for buildings equipped with linear and nonlinear viscous dampers. Engineering Structures, 78, 90-99.

[28] Tubaldi, E., Kougioumtzoglou, I.A., 2015. Nonstationary stochastic response of structural systems equipped with nonlinear viscous dampers under seismic excitation. Earthquake Engineering and Structural Dynamics, 44(1): 121–138.

[29] Dall'Asta, A., Tubaldi, E., Ragni, L., 2016. Influence of the nonlinear behaviour of viscous dampers on the seismic demand hazard of building frames. Earthquake Engineering and Structural Dynamics, 45(1), 149-169.

[30] Tubaldi, E., Ragni, L., Dall'Asta, A., 2015. Probabilistic seismic response assessment of linear systems equipped with nonlinear viscous dampers. Earthquake Engineering & Structural Dynamics, **44** (1), 101-120. DOI: 10.1002/eqe.2461
[31] Dall'Asta, A., Scozzese, F., Ragni, L., Tubaldi, E., 2017. Effect of the damper property variability on the seismic reliability of linear systems equipped with viscous dampers. Bulletin of Earthquake Engineering, 15(11), 5025-5053. DOI 10.1007/s10518-017-0169-8
[32] Lavan, O., Avishur, M., 2013. Seismic behavior of viscously damped yielding frames under structural and damping uncertainties. Bulletin of Earthquake Engineering, 11(6), 2309–2332.
[33] Scozzese, F., Dall'Asta, A., Tubaldi, E., 2019. Seismic risk sensitivity of structures equipped with anti-seismic devices with uncertain properties, Structural Safety, 77, 30-47.
[34] Miyamoto, H. K., Gilani, A. S., Wada, A., & Ariyaratana, C. (2010). Limit states and failure mechanisms of viscous dampers and the implications for large earthquakes. *Earthquake Engineering & Structural Dynamics, 39*, 1279-1297.
[35] Miyamoto, H. K., Gilani, A. S., Wada, A., & Ariyaratana, C. (2010). Collapse risk of tall steel moment frame buildings with viscous dampers subjected to large earthquakes: PART I: DAMPER LIMIT STATES AND FAILURE MODES OF 10- STOREY ARCHETYPES. The Structural Design of Tall and Special Buildings, 19(4), 421-438.
[36] Lee, D., & Taylor, D. P. (2001). Viscous damper development and future trends. The Structural Design of Tall Buildings, 10(5), 311-320.
[37] Agrawal, A. K., & Amjadian, M. (2016). Seismic component devices. In Innovative bridge design handbook (pp. 531-553). Butterworth-Heinemann.
[38] Filiatrault, A., & Christopoulos, C. (2006). Principles of passive supplemental damping and seismic isolation.
[39] Impollonia, N., & Palmeri, A. (2018). Seismic performance of buildings retrofitted with nonlinear viscous dampers and adjacent reaction towers. Earthquake Engineering & Structural Dynamics, 47(5), 1329-1351.
[40] Miyamoto, H. K., Gilani, A. S., Wada, A., & Ariyaratana, C. (2011). Identifying the collapse hazard of steel special moment-frame buildings with viscous dampers using the FEMA P695 methodology. Earthquake Spectra, 27(4), 1147-1168.
[41] Vamvatsikos, D., & Cornell, C. A. (2002). Incremental dynamic analysis. *Earthquake Engineering & Structural Dynamics*, 31(3), 491-514.
[42] Scozzese, F., Tubaldi, E., & Dall'Asta, A. (2020). Assessment of the effectiveness of Multiple-Stripe Analysis by using a stochastic earthquake input model. *Bulletin of Earthquake Engineering*, 1-37.
[43] Barroso LR, Winterstein S. Probabilistic seismic demand analysis of controlled steel moment-resisting frame structures. *Earthquake Engineering and Structural Dynamics* 2002; 31(12):2049–2066.
[44] Constantinou, M. C., & Symans, M. D. (1992). *Experimental and analytical investigation of seismic response of structures with supplemental fluid viscous dampers*. Buffalo, NY: National Center for earthquake engineering research.
[45] McKenna, F. (2011). OpenSees: a framework for earthquake engineering simulation. *Computing in Science & Engineering*, 13(4), 58-66.
[46] NTC 2018 (2018). Aggiornamento delle "Norme Tecniche per le costruzioni" (in italian). D:M: 17/01/2018 Ministry of Infrastructure and Transport.
[47] Ohtori, Y., Christenson, R.E., Spencer Jr., B.F. and Dyke, S.J. (2004). Benchmark Control Problems for Seismically Excited Nonlinear Buildings. *Journal of Engineering Mechanics*, 130, 366-385.
[48] Scozzese F, Terracciano G, Zona A, Della Corte G, Dall'Asta A, Landolfo R. Analysis of seismic non-structural damage in single-storey industrial steel buildings. Soil Dyn Earthq Eng 2018; 114:505–19. doi:10.1016/j.soildyn.2018.07.047.
[49] Scozzese F., Terracciano G., Zona A., Della Corte G., Dall'Asta A., Landolfo. R. (2017). RINTC project: Nonlinear dynamic analyses of Italian code-conforming steel single-story buildings for collapse risk assessment, COMPDYN 2017 - Proceedings of the 6th International Conference on Computational Methods in Structural Dynamics and Earthquake Engineering, M. Papadrakakis, M. Fragiadakis (eds.) Rhodes Island, Greece, 15–17 June 2017.
[50] Bradley BA. A comparison of intensity-based demand distributions and the seismic demand hazard for seismic performance assessment. Earthquake Engineering and Structural Dynamics 2013; 42(15):2235–2253.
[51] Occhiuzzi A. Additional viscous dampers for civil structures: analysis of design methods based on effective evaluation of modal damping ratios. Eng Struct 2009;31(5):1093–101.
[52] Seleemah, A.A. and Constantinou, M.C. (1997). *Investigation of seismic response of buildings with linear and nonlinear fluid viscous dampers.* Report No. NCEER-97-0004. New York: National Center for Earthquake Engineering Research, State University of New York at Buffalo.
[53] Hanson, R.D. and Song, T.T. (2001). *Seismic design with supplemental energy dissipation devices*. Oakland, California: Earthquake Engineering Research Institute.
[54] Gkimprixis, A., Tubaldi, E. & Douglas, J. *Comparison of methods to develop risk-targeted seismic design maps*. Bull Earthquake Eng 17, 3727–3752 (2019). https://doi.org/10.1007/s10518-019-00629-w